

Review

# The Effects of Size and Shape Dispersity on the Phase Behavior of Nanomesogen Lyotropic Liquid Crystals

Fatima Hamade , Sadat Kamal Amit , Mackenzie B. Woods  and Virginia A. Davis \* 

Department of Chemical Engineering, 212 Ross Hall, Auburn University, Auburn, AL 36849, USA; fzh0014@auburn.edu (F.H.); sza0111@auburn.edu (S.K.A.); mlb0061@auburn.edu (M.B.W.)

\* Correspondence: davisva@auburn.edu

Received: 7 July 2020; Accepted: 10 August 2020; Published: 18 August 2020



**Abstract:** Self-assembly of anisotropic nanomaterials into fluids is a key step in producing bulk, solid materials with controlled architecture and properties. In particular, the ordering of anisotropic nanomaterials in lyotropic liquid crystalline phases facilitates the production of films, fibers, and devices with anisotropic mechanical, thermal, electrical, and photonic properties. While often considered a new area of research, experimental and theoretical studies of nanoscale mesogens date back to the 1920s. Through modern computational, synthesis, and characterization tools, there are new opportunities to design liquid crystalline phases to achieve complex architectures and enable new applications in opto-electronics, multifunctional textiles, and conductive films. This review article provides a brief review of the liquid crystal phase behavior of one dimensional nanocylinders and two dimensional nanoplatelets, a discussion of investigations on the effects of size and shape dispersity on phase behavior, and outlook for exploiting size and shape dispersity in designing materials with controlled architectures.

**Keywords:** lyotropic liquid crystal; nanomaterial; mesogen; phase behavior

## 1. Introduction

The 130-year history of liquid crystal science is replete with examples of the discovery of new materials leading to advances in both fundamental science and breakthroughs in product development. Liquid crystals are mesophases that possess the fluidity of a liquid but the order of a solid. The building blocks of these phases are anisotropic materials with some rigidity known as mesogens. From 1888 through the 1950s, theoretical knowledge of liquid crystals advanced alongside the field of colloid science through empirical polarized microscopy investigations of naturally occurring materials such as cholesteryl benzoate, vanadium pentoxide, and tobacco mosaic virus (TMV). These observations led to the classification systems and seminal theories that still provide the foundation for modern liquid crystal research. Between the 1960s and 1970s, advances in chemical synthesis led to the production of materials such as 4-cyano-4'-pentylbiphenyl (5CB) and p-polyphenylene terephthalamide (PPTA). Notably, 5CB, a small molecule with a rigid core, is an example of a material that exhibits thermotropic liquid crystalline phase behavior. The discovery of thermotropic liquid crystals' ability to switch from disordered to ordered states with changes in temperature was the foundation for liquid crystal display technology. PPTA is a polymeric macromolecule whose aromatic rings impart rigidity. PPTA in sulfuric acid forms a lyotropic liquid crystal (LLC), a type of liquid crystal where the phase transitions are the result of changes in concentration. Fiber spinning of PPTA/H<sub>2</sub>SO<sub>4</sub> LLCs results in the highly aligned, high strength fibers known as Kevlar<sup>®</sup>. From the 1990s to date, scientists have been developing the ability to synthesize new anisotropic nanomaterials and more scalably isolate natural nanomaterials such as DNA, *fd* virus, and cellulose nanocrystals (CNC). Characterization of these materials' intrinsic properties and the desire to preserve their anisotropic properties in macroscale solid structures, such as

films and fibers, have resulted in a “new era for liquid crystal research” [1] that is focused on creating, understanding, and processing LLCs containing nanoscale mesogens. In many regards, however, the current nanotechnology-enabled lyotropic liquid crystal renaissance is based on a rediscovery of the field’s roots [2]. In the 1920s and 1930s, decades before scanning electron microscopes (SEMs) became widely used or Norio Taniguchi coined the term “nanotechnology”, Zocher reported the LLC phase behavior of aqueous vanadium pentoxide dispersions [3,4]. In 1935, Stanley first reported on the LLC phase formation of tobacco mosaic virus (TMV) [5]. The experiments conducted on TMV inspired the development of Onsager’s 1949 theory on LLCs which still serves as the foundation of the field [6]. In modern nomenclature, a nanomaterial is an object with at least one dimension less than 100 nm; both TMV and vanadium pentoxide fulfill this definition, and since they form liquid crystalline phases, they can be termed nanomesogens.

In general, there are two primary motivations for studying nanomesogen LLCs. First, nanocylinders, such as carbon nanotubes (CNTs) and inorganic nanowires, are much closer to fulfilling Onsager’s criterion for infinitely long rigid rods than the rod-like polymers that previously constituted the bulk of LLC research. The wide range of potential nanomesogen material sizes, densities, and surface chemistries provide new opportunities for advancing knowledge of the effects of size, shape, sedimentation, and thermodynamic interactions on phase behavior. Second, anisotropic nanomaterials provide new opportunities to produce bulk materials with anisotropic mechanical, electrical, thermal, and optical properties. The alignment in LLC phases facilitates manufacturing dispersions into highly aligned films, fibers, and electrical and optical devices that enable the nanoscale anisotropic properties to be manifested as bulk material properties. Processing nanomesogen LLCs is increasingly considered one of the most efficient methods for achieving aligned, large-scale, solid, assemblies of nanomesogens through manufacturing techniques such as solution spinning, film casting, and additive manufacturing. This combination of purely scientific and applied research opportunities has prompted several reviews highlighting how nanotechnology has enabled a renaissance in liquid crystal science and engineering [1,2,7,8].

The current review is focused on topics not yet widely discussed in the literature: the effects of size and shape dispersity on the phase behavior of lyotropic liquid crystals where one or more nanomaterials serve as the mesogen(s). From a scientific standpoint, many advances in these areas are relatively recent and there is still much to be understood. From an applications viewpoint, these are important topics because they can affect microstructure, processing, and performance properties of manufactured materials. Many nanomesogen syntheses or extraction schemes result in significant size polydispersity. Some, such as the polyol synthesis of silver nanowires, result in a mixture of shapes as well as sizes. Often, the unwanted shapes and sizes are removed through time-consuming separation techniques. However, it can also be desirable to exploit size or shape dispersity to tune the phase behavior, rheological properties, and performance properties such as thermal conductivity.

It is noted that in the interest of focusing the article, many important topics in nanomesogen LLC research are not described. This review only covers systems where a nanomesogen is in a non-mesogenic solvent; the equally important area of adding nanomaterials to known thermotropic or lyotropic liquid crystalline phases is not included. Additionally, the breadth of nanomaterial chemistries available means that detailed understanding requires considering the intersectionalities of size, shape, sedimentation, and non-athermal thermodynamic interactions. While sedimentation and non-athermal interactions are mentioned with respect to different systems, these topics are not discussed in detail. Also, while work from the 1980s and 1990s on nanoclays provide some theoretical insights, the complexities of sedimentation and thermodynamic interactions in dispersions of charged nanomesogens such as nanoclays, cellulose nanocrystals (CNC), MXenes, and other charged nanomesogen systems, are sufficiently complex to warrant a separate review.

## 2. Examples of Nanomesogens

Mesogens are materials that have the ability to form liquid crystalline phases; thus, nanomesogens are those for which at least one dimension is less than 100 nm. Such materials can be biological, naturally occurring, or synthesized; the main criteria are that they are anisotropic and can be classified as either “semi-flexible” or “rigid”. The definition of rigidity varies in the literature but is typically defined as the persistence length being greater than the contour length. While there are many interesting mesogen shapes and sizes, this review is focused on one-dimensional (1D) and two-dimensional (2D) nanomaterial mesogens. In the colloid and polymer literature, 1D materials are referred to as “spherocylinders,” “rigid-rods,” or “rod-like.” However, the term nanorod is commonly used for short solid cylinders and does not include the longer structures called nanowires or the hollow structures called nanotubes. Since the fundamental soft matter physics governing LLC phase behavior is based on their cylindrical shape, these materials will be collectively referred to as nanocylinders. Two-dimensional mesogens are referred to as sheets, plates, and platelets; for this review, the term nanoplatelet will primarily be used. Since zero-dimensional (0D) spherical nanoparticles often result from anisotropic nanomaterial syntheses and are sometimes intentionally added to some dispersions, they are also discussed in this review [9–12].

Investigation of nanomesogens began in the early 1900s, long before the prefix “nano-” became popular. Onsager’s seminal 1949 theory for LLC phase behavior was based on experimental observations of tobacco mosaic virus (TMV), a relatively monodisperse, rigid, biological nanocylinder of length  $L = 250$  nm and  $D = 15$  nm (aspect ratio  $L/D = 16.7$ ) [5,6,13]. An electron micrograph of TMV is shown in Figure 1. Biologically derived nanomesogens, such as *fd* virus, continue to serve as model experimental systems to aid theoretical advances [14]. Other biological nanomaterials such as cellulose nanocrystals (CNC) are more polydisperse, but their phase behavior is of interest for enabling the manufacture of anisotropic solid materials such as photonic films, high strength films, and fibers. Research on CNC liquid crystals began in the 1990s [15,16] and has recently gone through exciting advances spurred by increased material availability [17,18].

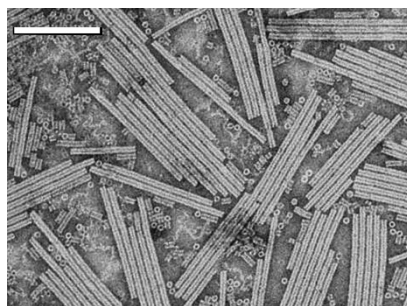


**Figure 1.** Electron micrograph of tobacco mosaic virus (TMV) on a substrate. Reprinted with permission from Fan, X.Z.; Pomerantseva, E.; Gnerlich, M.; Brown, A.; Gerasopoulos, K.; McCarthy, M.; Culver, J.; Ghodssi, R. Tobacco mosaic virus: A biological building block for micro/nano/biosystems. *J. Vac. Sci. Technol. A* 2013, 31, 050815 with the permission of AIP Publishing [19].

An even more historical area of LLC research that has been revived is mineral liquid crystals. Zocher first reported on vanadium pentoxide phase behavior in the 1920s. As of the early 2000s, there were very few mineral LLC systems that had been studied and most were nanoclays [20,21]. However, growing interest in nanomaterials such as MXenes and transition metal dichalcogenides (TMDCs) have not only prompted investigation of these materials but sparked a “fresh-look” [22] at the phase diagrams of nanoclays such as laponite and goethite [22–31].

Other actively researched nanomesogens are inorganic metallic semiconducting materials including oxides. Key examples include silver, gold, cadmium selenide (CdSe), germanium, zinc, tungsten, silica, zinc oxide, and manganese oxide. Research in this area has accelerated with

improvements in synthesis techniques and interest in bottom-up assembly of electronic devices through additive manufacturing methods. Many of these inorganic 1D nanomesogens can be synthesized with aspect ratios ranging from five to over a thousand [12,32–38]. CdSe can be considered a model material for studying the phase behavior of inorganic 1D nanomesogens because it was one of the first reported systems and can be produced with excellent monodispersity [34]. However, the synthesis of many other materials results in significant size, and sometimes shape, polydispersity. While time-consuming protocols, such as isopycnic centrifugation, can be used to improve the geometric consistency, both polydispersity and sedimentation effects make inorganic nanomesogens a fascinating class of materials for studying phase behavior. In addition, they are of significant interest for use in display technology, wearable electronics, electrochemical devices, and other opto-electronic applications [7].

Some of the most rapid advances in nanomesogen LLCs have been made in the subfield of carbon nanomaterial liquid crystals. It is now known that the sharpness and durability of Damascus swords were partially due to the presence of carbon nanotubes [39] and that small quantities of carbon nanomaterials can be obtained by simple processes such as lighting a candle or exfoliating pencil markings with sticky tape. However, in the year 2000, a mere gram of carbon nanotubes was considered a large quantity, graphene had yet to be “discovered”, and many doubted that carbon nanotubes could be dispersed at sufficiently high concentrations to form LLCs. However, during the last twenty years, liquid crystalline phases of pristine single-walled carbon nanotubes (SWNTs), multi-walled carbon nanotubes (MWNTs), and graphene in superacids have been discovered and applied to the production of aligned films and fibers [40–47]. In addition, favorable interactions with biomolecules such as DNA and hyaluronic acid as well as with  $\gamma$ -butyrolactone have resulted in LLC phase formation [48–51]. In addition, oxidized carbon nanomaterials such as graphene oxide (GO) can form liquid crystals in water and other solvents [41,52–61]. The combination of intrinsic properties and range of available solvents make carbon nanomaterials desirable mesogens for a range of applications including high strength materials, electrical conduits, electromagnetic interference shielding, thermal management, electrical devices, and biomedical materials.

### 3. A Very Brief Overview of Lyotropic Liquid Crystalline Phase Behavior

Based on mesogen orientational and positional arrangement, liquid crystals are categorized into four general classes: nematic, chiral nematic, smectic, or discotic. It should be noted that these arrangements are not static; a key criterion of liquid crystallinity is the ability to flow. In the nematic phase, mesogens possess a long-range orientational order but not positional order (Figure 2a). Their long axes align along a preferred direction, called director, with an order parameter  $S = (3\cos^2q - 1)/2$ , where  $q$  is the angle between the director and long axis of the mesogen. The chiral nematic, or cholesteric, mesophase is similar to the nematic phase but the director orientation twists along a perpendicular axis (Figure 2b). In contrast, in smectic mesophases such as the smectic A mesophase shown in Figure 2c, mesogens have both orientational and positional order where the layers of mesogens can freely slide over one another [7,62]. Two-dimensional platelet mesogens can also form a columnar or discotic phase shown in Figure 2d, where platelets stack into aligned columns [63].

There are two primary frameworks for discussing LLC phase behavior: Onsager theory and Flory theory. Flory theory is perhaps more widely known. Its applicability to polymer systems made it the foundation for research on so-called “rod-like” polymer mesogens, and it is a frequently covered topic in polymer and thermodynamic textbooks. However, many researchers have realized that the high aspect ratios and extreme persistence length to length ratios (28,500 for High Pressure Carbon Monoide [HiPCo] SWNT) better fit Onsager’s assumptions of infinite length and high rigidity. Since Onsager theory was based on observations of TMV nanocylinders, it should not be surprising that it provides the foundation for understanding nanomesogen phase behavior. Onsager’s original theory was based on the highly idealized scenario of monodisperse spherocylinders interacting through only hard rod repulsion; numerous subsequent refinements have been made into a robust framework that can account for polydispersity and thermodynamic interactions [45,64]. A cylindrical rod is a geometric

object of circular cross-section whose length  $L$  is much greater than its diameter  $D$  ( $L \gg D$ ). If one imagines compressing a cylindrical rod, it will form a disk (or platelet) with  $D \gg L$ ; however, it should be noted that many works use the convention that  $L$  is the lateral dimension of the platelet and  $D$  is the thickness. Therefore, the general elements of theories for the phase behaviors of 1D cylinders dispersed in a solvent are also applicable to 2D platelets; some caveats are discussed in Section 4.2. For clarity, the majority of discussion in this section is focused on 1D cylinders. In the absence of attractive or repulsive thermodynamic interactions when mesogens are dispersed in a solvent, their motion and alignment are solely dependent on their aspect ratio ( $L/D$ ) and their concentration. Figure 3 depicts the general behavior. At low concentrations, the cylinders are in a rheologically dilute phase where they can rotate and translate freely. Increasing the concentration initially constrains rotational movement (semi-dilute phase), and then confines both translational and rotational motion to straw-like volumes in the isotropic concentrated phase. Further increases in concentration result in some of the cylinders aligning because the resulting increase in translational entropy is greater than the corresponding decrease in rotational entropy. This occurs at a critical volume fraction  $\phi_I$  and results in a biphasic system where an anisotropic liquid crystalline phase exists in equilibrium with an isotropic phase. Further increases in concentration increase the fraction of the system that is liquid crystalline until at a second critical volume fraction  $\phi_{LC}$  the system becomes fully liquid crystalline [6,7,47,64–67]. For monodisperse cylinders interacting through hard-rod repulsion, the concentration of cylinders in each phase remains constant as the total concentration is increased. However, this is not the case for polydisperse or charged cylinders. In fact, the complexities of polydispersity, sedimentation, and thermodynamic interactions result in complex behaviors such as size fractionation, gelation, multiple forms of phase coexistence, and various forms of aggregation including the formation of crystal solvates. It should be noted that nanomesogen densities range from approximately  $1 \text{ g/cm}^3$  for organic materials to  $10 \text{ g/cm}^3$  for inorganic nanomaterials, and solvent densities can similarly range from  $\sim 0.7 \text{ g/cm}^3$  to over  $2 \text{ g/cm}^3$ . Even in the same solvent, organic and inorganic mesogens with the same aspect ratio will require significantly different masses of material to reach the same volume fraction. Therefore, while dispersions are often prepared by weighing the nanomaterial, it is important to consider the corresponding volume fraction which can be obtained from:

$$\phi = \frac{m_{nc}/\rho_{nc}}{m_s/\rho_s + m_{nc}/\rho_{nc}} \quad (1)$$

where  $m$  is the mass,  $\rho$  is the density, and the subscripts  $nc$  and  $s$  refer to the nanocylinder and solvent, respectively. This relation can be extended for multiple components. It should be noted that the densities of nanomaterials are often assumed from bulk values and can vary between sources; therefore, it is helpful when authors note what densities they used in their calculations.

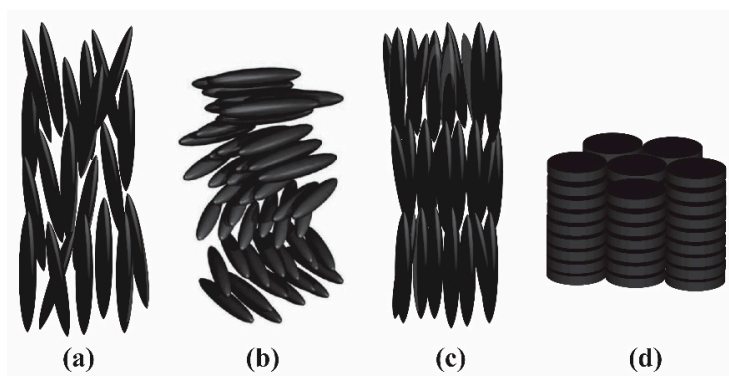


**Figure 2.** Schematic diagram representing the orientation of nanorods in (a) nematic, (b) cholesteric, (c) smectic A, and (d) discotic liquid crystalline phases.

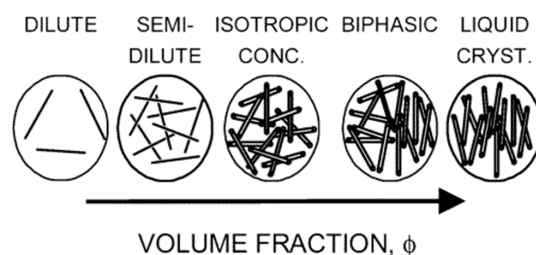


**Figure 3.** Phase behavior of dispersed rigid rods. Reprinted with permission from Davis, V.A.; Ericson, L.M.; Parra-Vasquez, A.N.G.; Fan, H.; Wang, Y.; Prieto, V.; Longoria, J.A.; Ramesh, S.; Saini, R.K.; Kittrell, C., et al. Phase Behavior and Rheology of SWNTs in Superacids. *Macromolecules* 2004, 37, 154–160. Copyright (2004) American Chemical Society [47].

For systems that closely obey Onsager's restrictions of monodispersity and only hard rod interactions, the phase boundaries are simply dependent on the aspect ratio,  $\phi_I = 3.34/(L/D)$  and  $\phi_{LC} = 4.43/(L/D)$ . However, for real systems, the phase behavior can be markedly more complex; this can be shown on a phase diagram with volume fraction on the  $x$ -axis and solvent quality or a related parameter on the  $y$ -axis. Figure 4 shows a representative phase diagram for a polydisperse cylindrical mesogen in a non-athermal solvent [68]. Both polydispersity and differences in mesogen–mesogen versus mesogen–solvent interactions can result in complex behaviors including multiple liquid crystalline phases, aggregation, kinetic arrest (gelation), and aggregates such as crystal solvates which possess the order of a liquid crystal but lack the ability to flow. As described in Section 4, polydispersity can lead to the coexistence of multiple liquid crystal phases. In addition, when the solvent is less favorable the width of the coexistence region can be quite broad, while for more favorable solvents it is a narrow region known as the biphasic chimney. For rod-like polymers, the solvent quality can be improved (mesogen–solvent interactions can be made more favorable) by simply increasing temperature. This equates to decreasing the well-known Flory–Huggins interaction parameter  $\chi$ . However, due to nanomesogens' typically greater length and rigidity, temperature is often an ineffective method of changing thermodynamic interactions and phase behavior of nanomesogen dispersions. For a given mesogen, the solvent quality can only be varied by changing the solvent itself. This is often achieved by using a mixture of liquids such as DMSO/water for silica nanorods [32] and sulfuric/chlorosulphonic acid for carbon nanotubes [69].

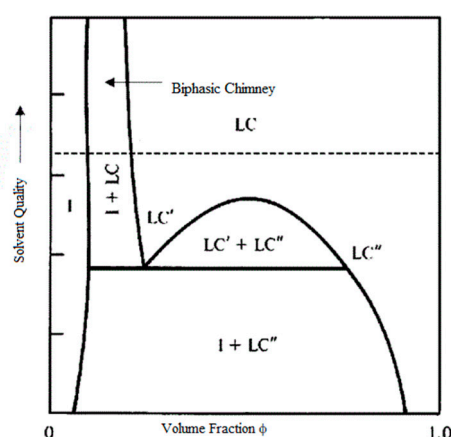


**Figure 4.** Generic phase diagram showing the biphasic chimney for favorable solvents, a broad coexistence region for less favorable solvents, and the potential for coexistence of multiple liquid crystalline phases. I: Isotropic, LC': one type of liquid crystal phase, LC'': another type of liquid crystal phase. Adapted with permission from Zhang, S.J.; Kinloch, I.A.; Windle, A.H. Mesogenicity drives fractionation in lyotropic aqueous suspensions of multiwall carbon nanotubes. *Nano Letters* 2006, 6, 568–572. Copyright (2006) American Chemical Society [68].

#### 4. Effects of Size Dispersity

Ever since Onsager's initial theory, experimental and computational researchers alike have wrestled with the impacts of size dispersity on phase behavior and the related topics of rheological behavior, processability, and properties of solid materials assembled from lyotropic liquid crystalline phases. Even after decades of refinement, most polymer syntheses result in a range of molecular weight distributions (and therefore length distributions). This affects not only phase behavior in fluid phase processing methods such as fiber spinning, but also chain alignment, crystallization processes, and mechanical properties. In polymers, the molecular weight (size) distribution is measured using techniques such as rheology, gel permeation chromatography, and light scattering. The various moments of the distribution are then represented in terms of the weight average  $M_w$ , number average  $M_n$ , and z-average  $M_z$ , which all reflect different moments of the distribution. Many polymer suppliers provide the polydispersity index (PDI) =  $M_w/M_n$ . For nanomaterials, size (as well as shape) polydispersity can be the result of synthesis or sonication, which is widely used to disperse 1D nanomaterials and exfoliate 2D nanomaterials. Nanomaterial sizes can be measured using methods such as atomic force microscopy (AFM), light scattering, and rheology; each of these methods has its advantages and disadvantages. While the most commonly used method is AFM, it rarely reflects the true size distribution impacting phase behavior due to the potential for aggregation in dispersions, biases resulting from sample preparation, larger objects being more visible and more likely to be manually measured, and the time required to count the thousands of objects required to obtain statistically meaningful results instead of the 100 or fewer objects typically counted. Software for automatic measurement can remove some of these issues [70], but as a method that requires drying the sample on a substrate it is never certain AFM truly reflects the size of the nanomaterial as it exists in the dispersion. For example, AFM samples prepared from dilute dispersions may show individual nanomaterials, but they may have a larger size in the dispersion of interest due to bundling or aggregation. Light scattering and rheology are both ensemble methods, but light scattering cannot capture larger objects and issues of optical opacity can be a challenge. In terms of rheology, Ubbelohde type capillary viscometers may produce erroneous results for rods because of flow alignment. Rotational rheometers can be limited by instrument sensitivity and the need for the material to meet stringent criteria such as behaving as Brownian rods [71]. Regardless of the method used, the size distributions can be quantified using similar metrics as the ones used for polymers (e.g., weight average length  $L_w$ , number average length  $L_n$ ).

A more complicated issue is the nature of nanomaterial size dispersity. A mesogen's length to diameter ratio ( $L/D$ ), known as the aspect ratio, is a fundamental determinant of LLC phase behavior. Different batches of a material can have very different aspect ratios. Even for the same batch, the aspect ratio can vary depending on the dispersion preparation method and changes due to aging. For example, length distribution of SWNTs in a dispersion is heavily dependent on sonication power, time, initial length, and stiffness [72]. Similarly, for CNC, length distribution depends on the source (e.g., wood, bacteria, tunicate), hydrolysis time, temperature and types of acid used to hydrolyze the cellulose to obtain CNC [73–75]. Another issue is deviations from a true cylindrical or disk shape. Some 1D nanomaterials, such as cellulose nanocrystals (CNC), have been found to generally obey the physics for dispersed spherocylinders, but they actually have three distinct dimensions and are perhaps more accurately described as lathes. The lateral dimension of some 2D nanomaterials such as the families of graphene-based and MXene materials are not smooth circular disks; this poses uncertainty in accounting for shape irregularity or their ability to wrinkle. Some researchers use more ideal materials such as *fd* virus [14,76] for comparison of theoretical developments with experiments. On the other hand, experimentalists working with polydisperse 1D and 2D systems are often reluctant to compare their results to theory, or if they do, they limit their comparisons to general concepts. For example, many experimental papers use average dimensions to calculate theoretical phase boundaries based on Onsager's original theory and then simply state that any discrepancies are the result of polydispersity and nanomesogen–solvent interactions. The sections below highlight the evolution of understanding the effects of size dispersity on phase behavior. They also describe that while monodispersity is

typically viewed as desirable, many researchers are using the phase behavior of polydisperse mesogens to achieve complex phase behaviors that cannot be obtained in monodisperse systems.

#### 4.1. Length Dispersity of 1D Materials

In general, rods of polydisperse lengths result in size fractionation, widening of the biphasic region [45,77,78], changes in the order parameter, and repressed smectic phase formation [77]. Diameter distribution also has some influence, but diameters are typically more uniform and length effects dominate the change in aspect ratio and phase behavior. The issue of length distribution is not new; even Onsager considered the potential impact of polydispersity. He correctly predicted that in a binary mixture of rod lengths, there would be a higher concentration of longer rods in the anisotropic phase. This prediction was confirmed by Oster who investigated mixtures of monodisperse TMV and end-to-end aggregated TMV [79]. Subsequent theoretical and experimental work on a wide variety of systems including 1D nanomesogens has confirmed the existence of size fractionation. In fact, some researchers have exploited this thermodynamically driven separation technique to obtain dispersions with lower polydispersity that could be processed into more uniform solid materials. For example, Honarato-Rios et al. found that by simply leaving aqueous biphasic dispersions of sulfated CNC in a separation funnel, the system would fractionate, and that repeating this process resulted in much lower polydispersity that enabled the production of more uniform optical films [80]. Similarly, Vroege et al. allowed highly polydisperse goethite nanorods to fractionate during sedimentation. Although polydisperse samples are generally deemed incapable of forming smectic liquid crystals, the resulting fractionation enabled the formation of different phases at different heights of the capillary. The nematic phase formed after approximately one week, while further fractionation resulting in the smectic phase did not occur for one month (Figure 5).

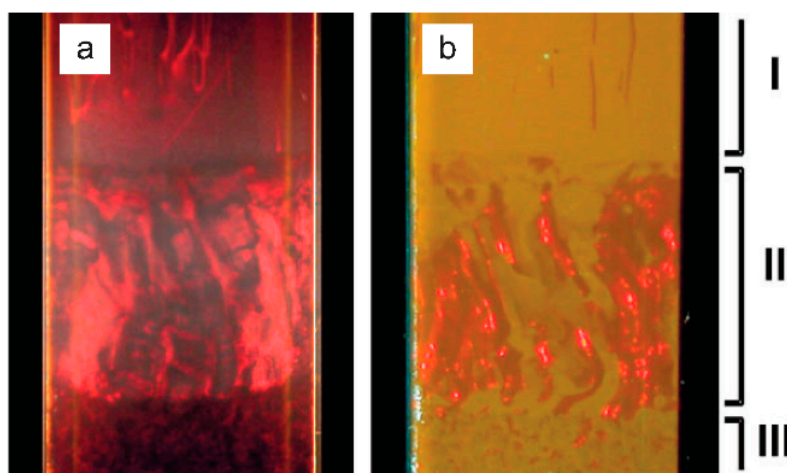


**Figure 5.** Capillary tube containing phase-separated goethite dispersions (16% volume fraction) displaying three distinctly different regions in addition to an isotropic region higher in the capillary (not shown). Images are taken using (a) transmitted light between crossed polarizers: Schlieren patterns typical for a nematic phase are observed in region I. (b) Reflected light: bright red Bragg reflections from a smectic phase are seen in region II. The columnar phase (predominant in region III) is not distinguished by special optical characteristics. Reprinted with permission from Vroege, G.J.; Thies-Weesie, D.M.E.; Petukhov, A.V.; Lemaire, B.J.; Davidson, P. Smectic Liquid-Crystalline Order in Suspensions of Highly Polydisperse Goethite Nanorods. *Advanced Materials* 2006, 18, 2565–2568. Copyright (2006) WILEY-VCH Verlag GmbH & Co. KGaA, Weinheim [23].

The example above also highlights how polydispersity can enable the coexistence of multiple liquid crystalline phases. Other work has also shown the complicated effects that vary with rod length [81]. Both Flory and Onsager based calculations have shown that significant size dispersity can

enable the formation of multiple liquid crystalline phases (including multiple nematic phases) without violating the Gibbs phase rule [82–85]. Experimentally, triphasic phenomenon has been observed in bidisperse systems of schizophyllan in water, polydisperse aqueous dispersion of boehmite rods, and bimodal solutions of imogolite [86–88].

Early work on evaluating the effects of size dispersity considered the relatively simple case of binary mixtures of two rods of the same density and diameter, but two different lengths  $L_b$  and  $L_a$  with  $m = L_b/L_a > 1$  [64,81]. If  $\phi_{2,a}$  and  $\phi_{2,b}$  are the volume fractions in the dispersion of rods of lengths  $L_b$  and  $L_a$ , then the overall rod volume fraction is  $\phi_2 = \phi_{2,a} + \phi_{2,b}$ . Defining  $z = \phi_{2,b}/\phi_2$ , the weight average length of the rods is:

$$\bar{L} = L_a(1-z) + L_bz \quad (2)$$

A reduced volume fraction can then be defined as  $\phi_r = \phi_2\bar{L}/d$ , where  $d$  is the diameter of the rod. This simple approach results in the well-known finding that polydispersity increases the width of the biphasic region by decreasing  $\phi_I$ , and increasing  $\phi_{LC}$  [64]. This effect is increased for greater values of  $z$ . It should be noted that this method results in only a small decrease in  $\phi_I$  and a large increase in  $\phi_{LC}$  [64], but experimental investigation of several nanomesogen systems have shown dramatic decreases in  $\phi_I$  and negligible increases in  $\phi_{LC}$ .

Most synthesized systems and systems extracted from larger materials (e.g., CNC, graphene) are not bidisperse but have continuous log-normal, Weibull, or Schultz distributions. For example, while typical commercial SWNT have a relatively narrow range of diameters, SWNT with an average length on the order of 700 nm, can contain a Weibull or log-normal distribution of lengths ranging from 100 nm to several microns. Even though continuous length distributions are common, it was not until the early 2000s that Onsager theory was adapted to account for such distributions. In 2002 and 2003, Speranza and Sollich used a simplified version of Onsager theory obtained by truncating the angular dependence of the excluded volume to calculate the effects of polydispersity on phase behavior. They used a moment free energy method to investigate a unimodal Schulz distribution, a bidisperse distribution, a bimodal mixture of two Schulz distributions, and log-normal distributions with a particular focus on the effects of “fat-tails” in the distribution [89–91]. In 2003, Wensink and Vroege published Onsager based results for Schulz and “fat-tailed” log-normal distributions using a Gaussian trial function ansatz. Both approaches resulted in biphasic regions greater than for monodisperse rods and three-phase I–N–N coexistence regions if the ratio of long and short rod lengths was sufficiently large. Green extended Wensink and Vroege’s approach by adding a square well potential to account for inter-rod attraction that could be varied based on the favorability of the dispersion of the solvent, a parameter termed solvent quality [45,69]. This approach enabled the first polydisperse nanomesogen phase diagram where the theoretical phase boundaries matched those obtained by experiment (Figure 6). As previously noted, unlike rod-like polymer liquid crystals, the size and rigidity of many nanomaterials cause temperature to be an ineffective method for tuning nanomaterial–nanomaterial and nanomaterial–solvent interactions and the resulting phase behavior. As a result, the phase diagram can only be obtained by changing the dispersant [32,69].

#### 4.2. Impact of Polydispersity on Phase Behavior of 2D Nanomesogens

As previously noted, 2D nanoplatelets are geometrically equivalent to short rods with lateral dimensions greater than their thicknesses. However, as pointed out by Onsager, applying his theory to infinitely short rods results in errors because of the truncation of the virial equation of state after the second virial term is justifiable for long rods, but not for disks [92]. The phase transitions for plates are often expressed in terms of dimensionless number densities  $nD^3$  which can be related to volume fraction  $\phi$  through  $nD^3 = 4\phi D^3/\pi D^2L$ . Applying Onsager theory to uniform disks interacting only through hard repulsion results in  $n_{iso}D^3 = 6.8$  and  $n_{nem}D^3 = 7.7$  for an aspect ratio  $D/L = 10$  and  $n_{iso}D^3 = 5.3$  and  $n_{nem}D^3 = 6.8$  for infinitely thin disks. However, Monte Carlo simulations using up to the fifth virial coefficient result in markedly lower values  $n_{iso}D^3 = 3.81$  and  $n_{nem}D^3 = 3.87$  for  $D/L = 10$  and  $n_{iso}D^3 = 4.04$  and  $n_{nem}D^3 = 4.12$  for infinitely thin disks [92].

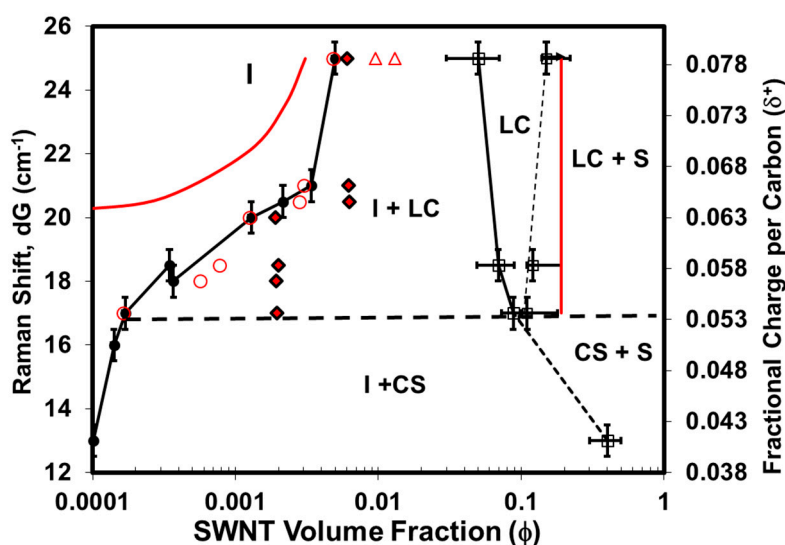


**Figure 6.** Phase diagram of single-walled carbon nanotubes (SWNTs) in mixtures of varying acid strengths showing isotropic (I), liquid crystal (LC), crystal solvate (CS), and solid (S) phases along with biphasic regions. Solvent quality is quantified by fractional charge per carbon, measured by the shift  $dG$  of the Raman G peak of SWNTs (514 nm laser). Onsager predictions for  $\phi_I$  and  $\phi_{LC}$  in a system of monodisperse hard rods are denoted by open red triangles. Black symbols denote experimental results and red symbols refer to model predictions. Circles designate  $\phi_I$  from experiment (filled circles) and model (open circles). Black and red diamonds indicate the initial system concentration before phase separation. Red lines are the model predictions of the isotropic and liquid–crystalline stability limits (cloud curves). Black dotted lines connect the experimental data points to denote phase boundaries. Modified with permission from Davis, V.A.; Parra-Vasquez, A.N.G.; Green, M.J.; Rai, P.K.; Behabtu, N.; Prieto, V.; Booker, R.D.; Schmidt, J.; Kesselman, E.; Zhou, W., et al. True solutions of single-walled carbon nanotubes for assembly into macroscopic materials. *Nature Nanotechnology* 2009, 4, 830–834. Nature Publishing Group [69].

Phase behavior of real 2D systems is complicated by several factors. While some are nearly uniform in size and have a regular shape, they may not be circular. For example, gibbsite is hexagonal. Sedimentation of these and other inorganic, or primarily inorganic, nanomaterials also complicates phase behaviors. As previously mentioned, materials such as graphene and MXene, which are produced by exfoliation, have high polydispersities in nominal size and highly irregular cross sections. These materials can also wrinkle, further changing their aspect ratio. In their study of aqueous graphene oxide (GO) dispersions, Jalili et al. obtained experimental values for the liquid crystalline phase transitions that were approximately five times higher than the predicted values and attributed this to wrinkling of the sheets [60]. Finally, many 2D nanomaterials such as nanoclays are charged and may exhibit complex phase behaviors as a function of ionic strength including isotropic, nematic, columnar, and gels [22,25,26,30,31,93].

There have been fewer investigations on the effects of polydispersity on the phase behavior of 2D nanomaterials than on 1D nanomaterials. Much of the early work was performed on nanoclays with more recent work on “newer” 2D nanomesogens only beginning to emerge. In general, the volume fraction of polydisperse platelets ( $\phi$ ) is

$$\phi = \frac{3\sqrt{3}}{8} \frac{L(1+\sigma)}{D(1+3\sigma^2)} (nD^3) \quad (3)$$

where  $\langle L \rangle$  is the average sheet thickness,  $\langle D \rangle$  is the average lateral size,  $\sigma$  is the polydispersity defined as the average diameter divided by the standard deviation of the diameter, and  $n$  is the number density of sheets per volume ( $N/V$ ) where the number densities for the isotropic and nematic phases are

designated as  $n_{iso}$  and  $n_{nem}$ , respectively [30,60,92,94,95]. In van der Kooij and Lekkerkerker's study of polymer stabilized gibbsite with  $\langle D \rangle / \langle L \rangle = 11$ , they obtained  $n_{iso} \langle D \rangle^3 = 2.5$  and  $n_{nem} \langle D \rangle^3 = 2.7$ . They attributed this discrepancy from the theoretical values of  $n_{iso} D^3 = 3.81$  and  $n_{nem} D^3 = 3.87$  for  $D/L = 10$  to three factors: polydispersity, gibbsite being hexagonally shaped, and gibbsite being slightly attractive [92].

Ahmad et al. explored the effects of changes in GO size, with increasing ultra-sonication time and the corresponding impacts on phase behavior. The GO diameter decreased from  $\sim 8 \mu\text{m}$  to  $\sim 0.1 \mu\text{m}$  over 9000 s (2.5 h) of ultrasonication (Figure 7a) [96]. Four different GO sheet sizes were used to investigate the effects of size on the concentrations (in wt%) at which the system became biphasic and liquid crystalline (Figure 7b) [96]. As expected, larger sheet sizes underwent the phase transitions at lower concentrations. Exploration of the effects of electro-optical sheet size on sensitivity showed that 2 wt% of the  $0.5 \mu\text{m}$  GO provided the fastest response time [96].

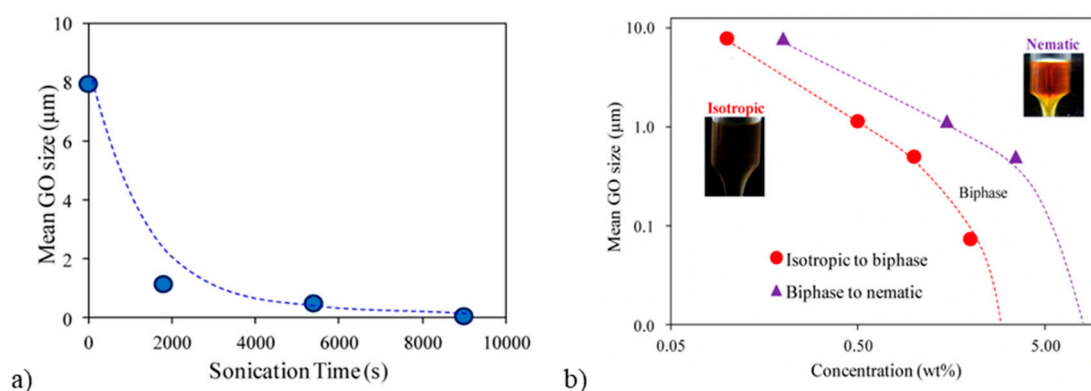


**Figure 7.** (a) Mean graphene oxide (GO) sheet size as a function of sonication time. (b) Comparison of isotropic to biphasic and biphasic to nematic phase boundaries of four different mean GO sheet sizes. Adapted and reprinted with permission from Ahmad, R.T.M.; Hong, S.-H.; Shen, T.-Z.; Song, J.-K. Optimization of particle size for high birefringence and fast switching time in electro-optical switching of graphene oxide dispersions. *Opt. Express* 2015, 23, 4435–4440 with the permission of AIP Publishing [96].

One of the most significant recent works highlighting the advantages of polydisperse systems is Jalili et al.'s exploration of the effects of size on aqueous GO dispersions' phase behavior, rheology, and ability to be wet spun into fibers [60,94]. For their ultra-large graphene oxide sheets with an average aspect ratio of 45,000, the dimensionless number densities were found experimentally to be  $n_{iso} D^3 = 2.7$  and  $n_{nem} D^3 = 4.3$  [60]. This corresponds to the biphasic region occurring theoretically between 0.05–0.09 mg/mL; however, polarized optical microscopy (POM) results portrayed that the nematic phase begins at 0.25 mg/mL [60]. They demonstrated the formation of liquid crystalline ultra-large GO with  $\langle L \rangle = 37 \pm 23 \mu\text{m}$  and  $\langle D \rangle = 0.81 \text{ nm}$  or an aspect ratio of 45,000 [60], which is much larger than the  $\sim 1,600$  aspect ratio typical for GO. They associated liquid crystalline phase formation with spinnability of dispersions into fibers [94]. They categorized aqueous 2.5 mg/mL GO dispersions with different average sheet sizes in terms of whether they were fully nematic ( $\phi_{nem} = 1$ ), biphasic ( $\phi_{nem} < 1$ ), or isotropic ( $\phi_{nem} \sim 0$ ). Figure 8a shows representative images of sheets from each category [94]. Average sheets size of  $3.2 \pm 6.9 \mu\text{m}$  and higher were more suitable for wet spinning due to their nematic microstructure. Interestingly, they found that mixing a small quantity of an isotropic dispersion of large ( $37 \pm 23 \mu\text{m}$ ) GO with an isotropic dispersion of small ( $0.2 \pm 0.15 \mu\text{m}$ ) GO resulted in a nematic liquid crystal (Figure 8b) due to the change in excluded volume. These dispersions were suitable for fiber spinning; this result highlights how intentional use of polydispersity can result in liquid crystalline phase formation and enable the production of aligned solid materials.

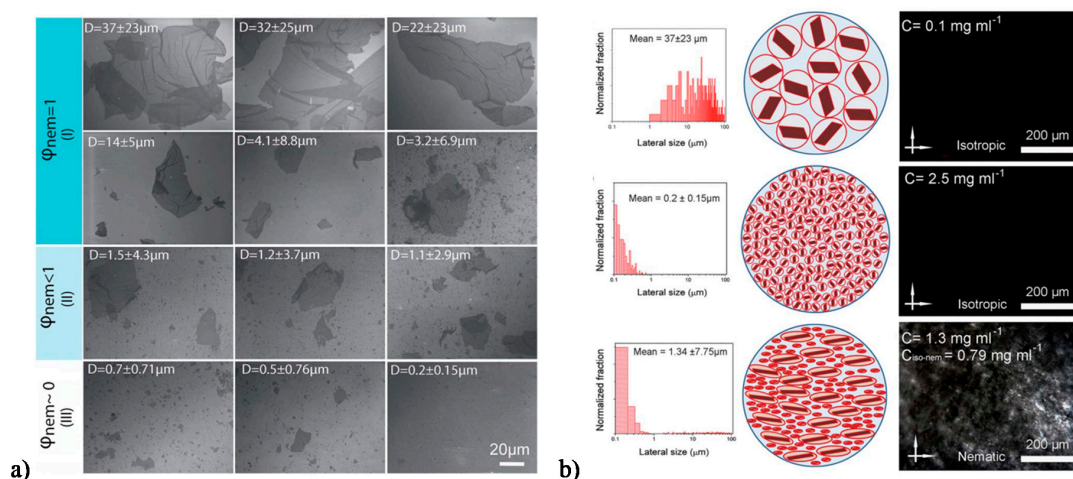


**Figure 8.** (a) SEM images examining the effect of ultra-large GO sheet size ( $D$  is lateral dimension) on wet-spinning capability, where (I), (II), and (III), represent spinnable, slightly spinnable, and non-spinnable. (b) Isotropic and non-spinnable ultra-large sheet (top) and small sheet GO (middle) can be combined to form a nematic liquid crystalline dispersion suitable for fiber spinning. Modified with permission from Jalili, R.; Aboutalebi, S.H.; Esrafilzadeh, D.; Konstantinov, K.; Razal, J.M.; Moultona, S.E.; Wallace, G.G. Formation and processability of liquid crystalline dispersions of graphene oxide. *Material Horizons* 2014, 1, 87–91, The Royal Society of Chemistry [94].

#### 4.3. Outlook for Understanding and Exploiting Polydispersity

The few results described in this section highlight that polydispersity has a significant impact on LLC phase behavior and while computer models based on Onsager's original theory show similar findings in many cases, the approach and definition of the distribution function can yield different results. The results also show how polydisperse systems can lead to desirable phase behaviors and facilitate processing methods such as fiber spinning. The current challenge is three-fold: (1) to further refine these theories to account for complex thermodynamic interactions, including effects of ionic strength, (2) be able to account for shape irregularity in 2D systems, and (3) increased control over nanomesogen synthesis and purification processes to enable producing materials with the size distribution needed to yield a desired phase behavior.

### 5. Effects of Shape Dispersity

While less inherent than nanomaterial size dispersity, shape dispersity is an important topic of increasing interest. Synthesis schemes can result in multiple shapes. For example, inorganic nanocylinder syntheses can result in the formation of conical materials, cubes, or spheres. Shape polydisperse dispersions can be considered as hypercomplex fluids that exhibit emergent properties unachievable by other means [97]. These properties can also be intentionally tuned to stabilize dispersions, modify rheological characteristics, enable multi-component dispersions of materials that are typically produced from different shapes, or achieve desired performance properties in fibers, coatings, and devices. For example, including 1D or 2D nanomesogens in dispersions of 0D nanoparticles can increase the thermal or electrical conductivity of devices by bridging microstructural gaps [35]. However, even when the same material is used, dispersions containing multiple shapes exhibit complex phase behaviors that need to be better understood for their potential to be exploited in engineering applications. This section reviews theoretical and experimental findings for binary mixtures of 0D nanoparticles, 1D nanocylinders, and 2D nanoplatelets. The additional complexities of mixing different types of materials with different densities and thermodynamic interactions of ternary and higher mixtures have been largely unaddressed in the literature but provide an intriguing area for future study.

### 5.1. Nanocylinders and Nanoparticles (1D–0D)

As well described in the broader colloid literature, polymers, surfactants, and biomolecules are often used to stabilize dispersions by retarding van der Waals attraction either by inducing electrostatic repulsion or steric hindrance. However, this effect is very concentration dependent. At higher concentrations, these materials can actually cause phase separation due to depletion attraction. Depletion forces were first described by Asakura and Oosawa in 1954 [98]. In essence, when small particles of diameter  $\sigma$  are added to a dispersion of larger objects, they are excluded (or depleted) from the gaps between larger objects when  $h < \sigma$  where  $h$  is the separation distance [99]. This results in the presence of only solvent between the larger objects and an osmotic pressure on the larger objects. The particles can be solid materials or soft materials such as polymers, surfactants, or globular proteins. For example, the globular protein lysozyme ( $D < 90$  Angstrom) is highly effective at dispersing nanocylindrical SWNT ( $D \sim 1$  nm,  $L \sim 500$  nm) in water. This is due to lysozyme's ability to adsorb on the SWNT sidewalls via  $\pi$ - $\pi$  interactions. However, increasing the concentration of free lysozyme which is not bound to SWNT results in the formation of large SWNT aggregates due to depletion forces driving the SWNT so close together that the van der Waals attraction between them causes large aggregates [100]. However, in cases where there are not strong thermodynamic attractions between 1D colloidal materials, depletion can actually stabilize liquid crystal phase formation by increasing the local concentration above that needed for liquid crystal phase formation. The concept of depletion is a recurring theme in both experimental and computational studies of nanomesogen dispersions. It is noted that while the addition of thin nanocylinders or platelets to dispersions of spheres can result in depletion [99,101,102], this section is primarily focused on the effects of adding spheres on the potential liquid crystalline phase formation in dispersions of nanocylinders.

In 2000, Dogic et al. published results of studying the phase behavior of spherocylinder-sphere (1D–0D) mixtures with Monte Carlo simulations [103]. In their model, each type of material was monodisperse, the spherocylinders were perfectly aligned, the orientational distribution function of the spherocylinders could not be disrupted by the presence of the spheres, and there were only hard interactions. Figure 9 illustrates the possible phases that can form from a nanocylinder–nanoparticle mixture. The miscible nematic phase includes a large excluded volume (gray areas) between the nanocylinders and nanoparticles (Figure 9a), the lamellar phase inhibits motion of the nanoparticles between the spherocylinders (Figure 9b), and the immiscible nematic or demixed system consists of spherocylinder-rich phase and sphere-rich phase (Figure 9c). Using a second virial approximation, the free energy difference between the uniformly mixed and layered states can be expressed as

$$\delta F = a_1^2 \left( S_{11} - 2 \frac{a_1}{a_2} S_{12} + \left( \frac{a_1}{a_2} \right)^2 S_{22} \right) = 0 \quad (4)$$

where  $S_{11}$  is the sphere–sphere interaction term,  $S_{22}$  is the rod–rod interaction term,  $S_{12}$  is the rod–sphere interaction term, and  $a_1$  and  $a_2$  are the amplitudes of fluctuation. The ratio of the amplitudes from Equation (4) is expressed as

$$\frac{a_1}{a_2} = - \frac{S_{12}(\eta_c, k_c)}{S_{11}(\eta_c, k_c)} \quad (5)$$

where  $\eta_c$  represents a specific total volume fraction and  $k_c$  represents a specific wave vector. A positive amplitude ratio is indicative of spheres and spherocylinders comprising the same layer, while a negative amplitude ratio is indicative of their intercalation [103].

Which phase forms depends on four parameters: the spherocylinder aspect ratio  $(L/D)_{sc}$ , the ratio of the spherocylinder and sphere diameters  $(D_{sc}/D_{sp})$ , the total volume fraction of spheres and spherocylinders ( $\eta$ ), and the partial volume fraction of spheres ( $\rho_{sp}$ ) [103]. Greater spherocylinder aspect ratio  $(L/D)_{sc}$  increases the tendency for the lamellar phase to form at a lower volume fraction of spheres. Second, if the spherocylinder diameter is greater than the sphere diameter ( $D_{sc}/D_{sp} > 1$ ), decreasing the sphere diameter increases stability of the lamellar phase. Third, for low aspect ratio

spherocylinders and larger diameter spheres (smaller  $L/D_{sc}$  and  $D_{sc}/D_{sp} < 1$ ), the spheres promote the formation of a demixed nematic because they cannot fit between the spherocylinders. However, for higher aspect ratio of spherocylinders the transition from the lamellar to demixed phase requires greater sphere diameter. Figure 10 shows two examples resulting from the work of Dogic et al. [103].

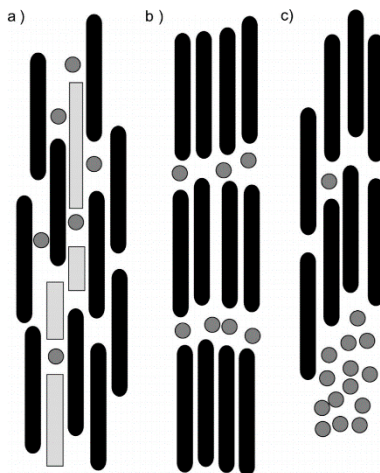


**Figure 9.** Illustrations of the (a) miscible (nematic) phase, (b) lamellar (layered) phase, and (c) immiscible phase. Reprinted with permission from Dogic, Z.; Frenkel, D.; Fraden, S. Enhanced stability of layered phases in parallel hard spherocylinders due to addition of hard spheres. *Physical Review E* 2000, 62, 3925–3933. Copyright (2000) by the American Physical Society [103].

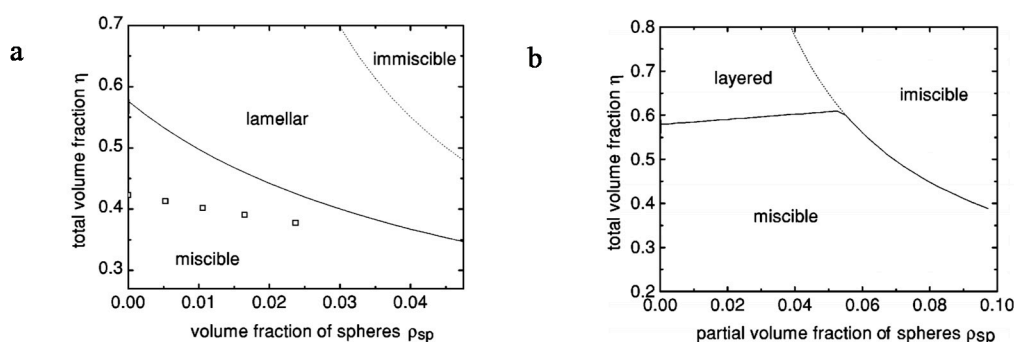


**Figure 10.** Phase diagrams of mixtures of spherocylinders ( $L/D_{sc} = 20$  and  $D_{sc}/D_p = 1$ , squares are results of computer simulations at which the lamellar transition is observed (a) small or (b) example effects of large diameter spheres for  $L/D_{sc} = 10$  and  $D_{sc}/D_{sp} = 0.15$ . Reprinted with permission from Dogic, Z.; Frenkel, D.; Fraden, S. Enhanced stability of layered phases in parallel hard spherocylinders due to addition of hard spheres. *Physical Review E* 2000, 62, 3925–3933. Copyright (2000) by the American Physical Society [103].

Adams et al.'s investigation of the phase behavior of *fd* virus (a nanocylinder) and polymer nanoparticles generally agreed with the results of Dogic et al.'s simulations [103,104]. Adams et al. first explored adding polystyrene spheres of  $D_s = 22$  nm at 5 vol%, to nematic dispersions of *fd* virus ( $L_{sc} = 880$ ,  $D_{sc} = 6.6$ ) in Tris buffer ( $20 \text{ mg ml}^{-1}$ , 10 mM Tris). This resulted in bulk demixing into a nematic nanocylinder-rich and isotropic nanocylinder-poor phase. The spheres partitioned into the isotropic phase and formed ellipsoidal shaped droplets whose long axes were parallel to the nematic director (rod alignment axis). Sphere concentrations above 700 nM resulted in complete demixing of the spheres into aggregates, which also elongated along the nematic director. The introduction of larger (100 nm) nanoparticles resulted in the complex phase behavior shown in Figure 11 [104]. Similar behavior was observed using a broad range of other diameters, but the required concentrations

for each phase varied. The columnar phase was not expected and only present for  $60 \text{ nm} < D_s < 120 \text{ nm}$ . In addition, in contrast to theory, the lamellar phase did not form for  $D_s > 250 \text{ nm}$ , and low concentrations of  $300 \text{ nm}$  nanoparticles resulted in the spheres rapidly associating into chain-like structures.

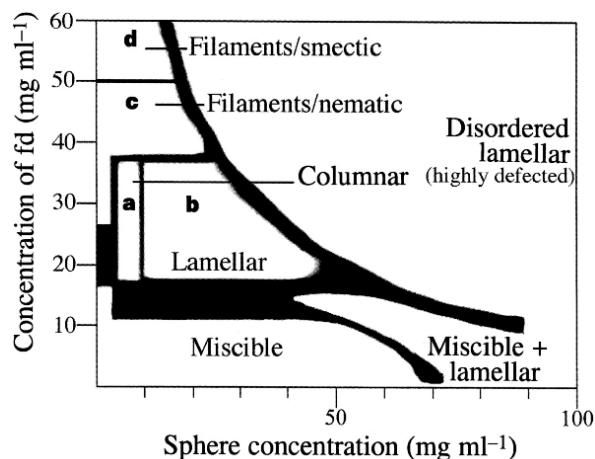


**Figure 11.** Phase diagram for *fd* virus and  $100 \text{ nm}$  polystyrene spheres. Reprinted with permission from Springer Nature: Nature, Entropically driven microphase transitions in mixtures of colloidal rods and spheres, Adams, M.; Dogic, Z.; Keller, S.L.; Fraden, Copyright (1998) [104].

TMV has also been used to understand the phase behavior of mixtures of 1D and 0D nanomesogens. For example, Urakami et al. performed Monte Carlo simulations on rods and spheres in an effort to understand changes in aqueous TMV phase behavior with the addition of chondroitin sulfate (Chs) and polyethylene oxide (PEO) where the Chs was treated as large spheres and PEO was treated as small spheres [105]. Their results generally agreed with the previously described results of Dogic et al. [103], as well as experimental studies [105]. Adams and Fraden [76] studied mixtures of TMV and the roughly spherical macromolecules bovine serum albumin (BSA), and polyethylene oxide (PEO) in  $50 \text{ mM}$  sodium borate buffer (ionic strength  $7 \text{ mM}$ ) with a pH of  $8.5$ . The spherical molecules acted as depletants and the researchers found a complex phase diagram that included isotropic, nematic, lamellar, and crystalline phase. These results also generally agreed with Dogic et al. [103].

More recent work on developing phase diagrams for 1D–0D mixtures has included inorganic nanomaterials. For example, Bakker et al. studied silica nanorods and nanoparticles [9]. Their results indicated the spontaneous formation of a binary smectic liquid crystalline phase, which they notate as  $\text{Sm}_2$ . This smectic phase was first observed by Adams and Fraden [76] with the *fd* virus. Bakker et al. expanded on this finding to show that stabilization was the result of entropy alone. Both experiments and simulations were used to understand the formation of this binary liquid crystalline phase. Experimentation on the sedimentation–diffusion equilibria of the mixture showed hard particle separation when in equilibrium, where most of the nanocylinders occupied the bottom portion and most of the nanoparticles occupied the top portion. The middle of the mixture consisted of both nanocylinders and nanoparticles, where a  $\text{Sm}_2$ -phase was ultimately formed as small domains. It was confirmed that entropy alone stabilized the domains when the  $\text{Sm}_2$ -phase remained stable after having a small AC-electric field applied to it and then removed.

In other work, the Davis group studied liquid crystalline phase behavior and aligned coatings from silver nanomaterials produced via the microwave-assisted polyol method [12,106]. As shown in Figure 12a, the synthesis resulted in a mixture of nanowires with  $\langle L_{sc} \rangle = 4.8 \mu\text{m}$  and  $\langle D_{sc} \rangle = 170 \text{ nm}$  ( $\langle L/D \rangle_{sc} \sim 80$ ) where *sc* indicates spherocylinders. However, while the relative mass and volume fraction of the nanowires was quite high, the number fraction of the nanowires was only  $0.05$ ; the remainder of the material was roughly spherical aggregates with  $D_{sp} = 170 \text{ nm}$  where *sp* indicates the roughly spherical aggregates [106]. In ethylene glycol (EG), the system transitioned from isotropic to biphasic

at a total silver concentration of  $\phi_I = 0.10$  vol% and formed a fully demixed nematic at  $\phi_{LC} = 0.42$  vol% total silver. The lyotropic phase behavior was evaluated using a combination of cross-polarized microscopy, rheology, differential scanning calorimetry and changes in the microstructure resulting from applied shear [12,106]. The authors hypothesized that the larger diameter of the spherical aggregates enabled formation of a demixed nematic at an order of magnitude lower concentration than the value of 4.8 vol% predicted by Onsager theory for monodisperse spherocylinders [12]. In cross-polarized optical microscopy images of the dispersions, the nanocylinders tended to sit above the spheres. Shearing and drying the sample increases this segregation and results in aligned silver nanowires sitting on a bed of packed nanoparticles (Figure 12b). The hypothesis of demixed nematic phase formation in the silver system led Green to develop a modified Onsager theory for mixtures of nanoparticles and length-polydisperse nanocylinders [107]. The experimental work by Murali et al. [12] was used to estimate the input data in the modeling parameters. However, the theoretical results were not in agreement with the experimental ones [107]. Instead, Green's model found that in mixtures with high nanocylinder length polydispersity, adding a small amount of monodisperse nanoparticles will increase length fractionation during phase separation, enabling ease of obtaining a near-monodisperse nanocylinder dispersion. Similar to Dogic et al. [103], Green found that  $D_{sc}/D_{sp}$  was a critical determinant of phase behavior highlighting that this parameter can be tuned to achieve desired phase behaviors.

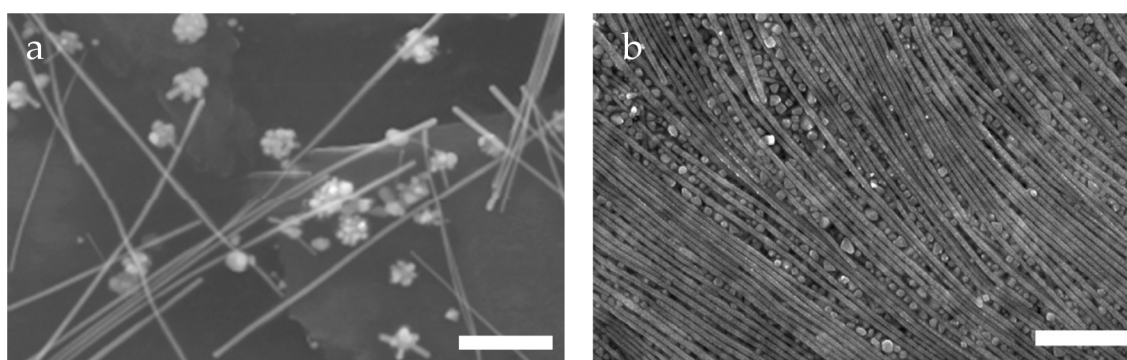


**Figure 12.** Scanning electron micrographs of silver nanomaterials produced by the microwave assisted polyol method (a) nanowires and spherical nanoparticle aggregates, (b) after shear the demixed nematic forms more aligned wires on a surface of packed nanoparticles. Scale bars are 1  $\mu\text{m}$ . Adapted with permission from Murali, S.; Xu, T.; Marshall, B.D.; Kayatin, M.J.; Pizarro, K.; Radhakrishnan, V.K.; Nepal, D.; Davis, V.A. Lyotropic liquid crystalline self-assembly in dispersions of silver nanowires and nanoparticles. *Langmuir* 2010, 26, 11176–11183 American Chemical Society [12].

In summary, fundamental colloidal theories and simulation methods are very beneficial for gaining insights into the phase behavior of nanocylinder–nanoparticle systems. However, even for relatively ideal systems such as *fd* virus and polystyrene nanoparticles, the experimental phase diagrams can be even richer than those predicted from simulations [9,103,105,107–110]. The complexities of shape disperse mesogens are further complicated by length polydispersity and attractive interactions. For inorganic materials, sedimentation resulting from the mesogen density being much greater than that of the solvent likely also plays a role. Further theoretical, computational, and experimental work are needed to fully understand these issues and dictate dispersion microstructure through dispersion formulation.

### 5.2. Nanoplatelets and Nanoparticles (2D–0D)

The addition of 0D nanoparticles to 2D nanoplatelets is of interest because it can retard gelation [10] and facilitate processing. It has been studied using simulations based on the Parsons–Lee theory [111], density functional theory [112] and the free-volume scaled-particle approach [113]. Oversteegen and

Lekkerkerker [113] used a free-volume theory that employed a hypothetical reservoir in which the particles and platelets mixture was contained and considered the available system volume for the colloidal mixture. The scaled-particle theory was used to determine the free-volume fraction available to the platelets in the systems through  $\alpha = e^{\frac{-W}{k_b T}}$  where  $\alpha$  is the free-volume fraction, and  $k_b T$  is the thermal energy.  $W$  is the insertion work determined by using particle size limits which ultimately reduce to finding the excluded volume of a platelet around a particle. The calculations performed by Oversteegen and Lekkerkerker [113] suggested that isotropic–isotropic demixing into particle-rich and platelet-rich regions would occur when the radius ratio of the particles to platelets is  $R_{particle}/R_{platelet} < 2.44$ . Harnau and Dietrich [112] obtained a similar result of  $R_{particle}/R_{platelet} = 2$  using density functional theory (DFT). A geometry-based DFT was later used by de las Heras and Schmidt to study more complex and liquid crystalline phase behavior of colloidal particles and infinitely thin platelet mixtures with varying sizes of materials [114]. Unlike the previously mentioned work, de las Heras and Schmidt accounted for the excluded-volume interactions which play a large role in microstructure and phase behavior at low concentrations. They defined  $F = F_{id} + F_{exc}$  where  $F_{id}$  is the ideal part and  $F_{exc}$  is the excess part. The platelets to particle size ratio was found to be the main parameter controlling the system's phase behavior. When the ratio is  $0.2 \leq R_{platelet}/R_{particles} < 10$  only an isotropic–nematic phase separation was seen. When the particle volume fraction is low, the excluded-volume interaction between the platelets drives the isotropic–nematic phase transition. If the particles volume fraction is high, the interaction between the particles and platelets becomes the driving force, and strong demixing between a particle-rich isotropic phase and a platelet-rich nematic phase occurs. When the  $R_{particle}/R_{platelet} > 10$ , then demixing of two nematic phases occurs.

Chen et al. experimentally explored the phase behavior of mixtures of monolayer zirconium phosphate (ZrP) platelets and silica spheres. The polydispersities of the platelets and spheres were 0.13 and 0.17, respectively. It is known that polydispersity increases the width of the I–N coexistence region for platelets. However, as noted by the authors, the effects of polydispersity in a mixed shape system was an open question which had not yet been resolved by theory or experiment [10]. The authors showed that the presence of the silica spheres retarded gelation, and higher concentrations of spheres reduced the time required to achieve I–N coexistence [10]. Sedimentation resulted in changes in the dispersion over the thirty days of study. They also observed  $I_1$ – $I_2$  and  $N_1$ – $I_1$ – $I_2$  phase coexistence (Figure 13a). They placed their experimental results on a graph showing results from other works (Figure 13b). In conclusion, they noted, “The exact boundary between N–N and I–I demixing still awaits for further experimental and theoretical investigations.” [10].

This knowledge gap was partially addressed less than one year later by Aliabadi et al.'s investigation of mixtures of hard platelets and particles [111]. In contrast to much of the previous literature, they assumed the plates had finite thickness  $L$  instead of being infinitely thin. Using the Parsons–Lee theory the free energy  $F$  can be found from:

$$\frac{\beta F}{V} = \sum_{i=p,s} \rho_i (\ln \rho_i - 1 + \sigma[f_i]) + \frac{4-3\eta}{8(1-\eta)^2} \times \sum_{i,j=p,s} \rho_i \rho_j V_{exc}^{ij}[f_i, f_j] \quad (6)$$

where  $\beta$  is the inverse temperature,  $V$  is the system volume,  $\rho$  is the density of the respective component,  $\eta$  is the volume fraction of the system,  $\sigma[f_i]$  is the orientational entropy term, and  $V_{exc}^{ij}[f_i, f_j]$  is the excluded volume entropy term. They expressed the relevant size ratios as  $d = \sigma/D$  and  $k = L/D$  where  $\sigma$  is the spherical particle diameter,  $D$  is the lateral diameter of the platelet, and  $L$  is the thickness of the platelet. They explored  $0.001 < k < 0.1$  to cover the range of thin materials such as laponite as well as thicker platelets. Phase diagrams of the fraction of the spheres  $\eta_s$  versus the fraction of platelets  $\eta_p$  are shown in Figure 14a–c for  $\sigma/D = 1.3, 0.2, \text{ or } 0.03$  (note this is equivalent to  $R_{sphere}/R_{platelet}$  or  $R_{particle}/R_{platelet}$  used in other works). While the differences in the axes' scales used make direct visual comparison difficult, noteworthy differences are the existence of a narrow  $I_1$ – $I_2$  phase and  $N_1$ – $I_1$ – $I_2$  phase for  $\sigma/D = 1.3$  and  $N_1$ – $N_2$  and  $N_1$ – $N_2$ – $I$  phases for  $\sigma/D = 0.03$ . Figure 14d further highlights the complexity

of the phase diagram by plotting  $d$  versus  $k$ . The authors noted that polydispersity, non-uniform charge distribution, and sedimentation could affect the results for experimental systems but included some experimental points on the phase diagram to help validate their results. In particular, they noted that their findings agreed with Chen et al.'s experimental results on demixing [10,111].

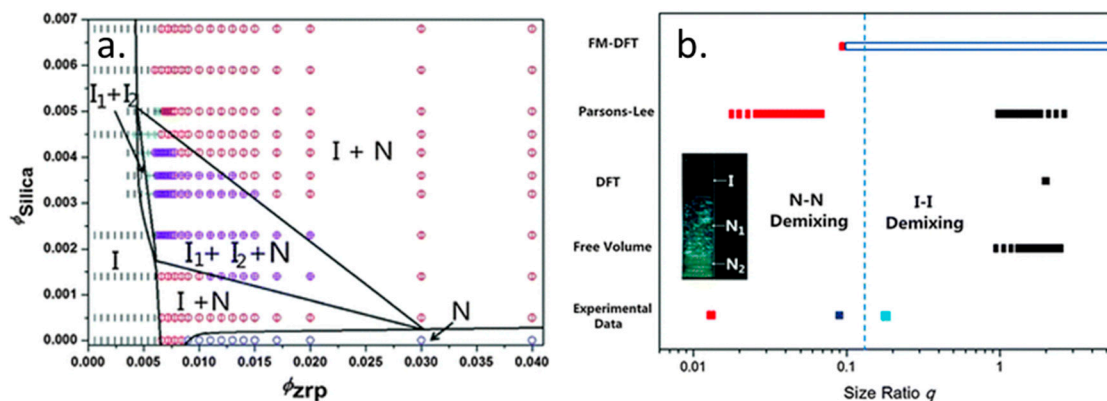


**Figure 13.** (a) Phase diagram as a function of ZrP plate and silica sphere concentrations. (b) The distribution of nematic–nematic demixing and isotropic–isotropic demixing found from several different theoretical frameworks as well as experimental data, as a function of size ratio  $q$  where  $q = R_{particle}/R_{platelet}$ . The dark blue squares give the bar size ratio in experiment and the light blue squares gives the effect size ratio accounting for ion clouds. The red square is the experimental observation of  $I-N_1-N_2$  demixing at  $q \sim 0.013$ . The long empty rectangle box stands for neither  $I_1-I_2$  nor the  $N_1-N_2$  demixing, while the solid red rectangle stands for  $N_1-N_2$  demixing, and the solid black rectangle stands for the  $I_1-I_2$  demixing. Dashed rectangles indicate that the limit valve has yet to be determined. The vertical dotted line indicates the possible boundary between  $I_1-I_2$  and  $N_1-N_2$  demixing. Reproduced with permission from Chen, M.; Li, H.; Chen, Y.; Mejia, A.; Wang, X.; Cheng, Z. Observation of isotropic–isotropic demixing in colloidal platelet–sphere mixtures. *Soft Matter* 2015, 11, The Royal Society of Chemistry [10].

Another issue in nanoplatelet–nanoparticle phase behavior briefly explored by Chen et al. [10] is temporal changes resulting from sedimentation. This was studied in more detail by Kleshchaok et al. for gibbsite nanoplatelets and silica nanoparticles [115]. The gibbsite was  $D_{plate} = 232.5$  nm,  $L_{plate} = 8.4$  nm and the silica had diameter  $D_{particle} = 16.8$  nm. The particles and platelets had the same charge sign to induce strong depletion attraction between them. In previous work, the authors had shown that this system did not form a liquid crystalline phase on short time scales [24]. Samples of either 4 vol% or 8 vol% gibbsite and ranging through 2, 3, 5, 7, and 8 vol% of silica were prepared and left to sediment for a year. The results are shown in Figure 15. A columnar phase formed after only one month in the samples with  $<7$  vol% silica particles. The samples with  $\geq 7$  vol% silica particles had no columnar phase formed after one year of sedimentation. The size of the columnar phase region was dependent on particle volume fraction; it decreased with increasing particle concentration. Sui addressed the issue of sedimentation in platelet–particle colloidal mixtures from a theoretical perspective and used a minimal energy model to further study the sedimentation dynamics of particle–platelet colloidal mixtures, specifically the shape stratification that occurs in nematic phases of the particle–platelet mixtures [116]. Similar to the results of previous work, Sui found that both the volume fraction of particles and the size ratio of the two types of mesogens have large effects on the nematic stratification structure. When the size ratio is  $R_{particle}/R_{platelet} \leq 0.3$ , the nematic platelet-rich regions falls to the bottom of the sedimented mixture; however, when  $R_{particle}/R_{platelet} \geq 0.4$ , the nematic platelet-rich region floats on top as a result of excluded volume interactions that push the platelets upward above sedimenting particles. Between these two values, which the phase forms depend on the concentration of spheres [116].

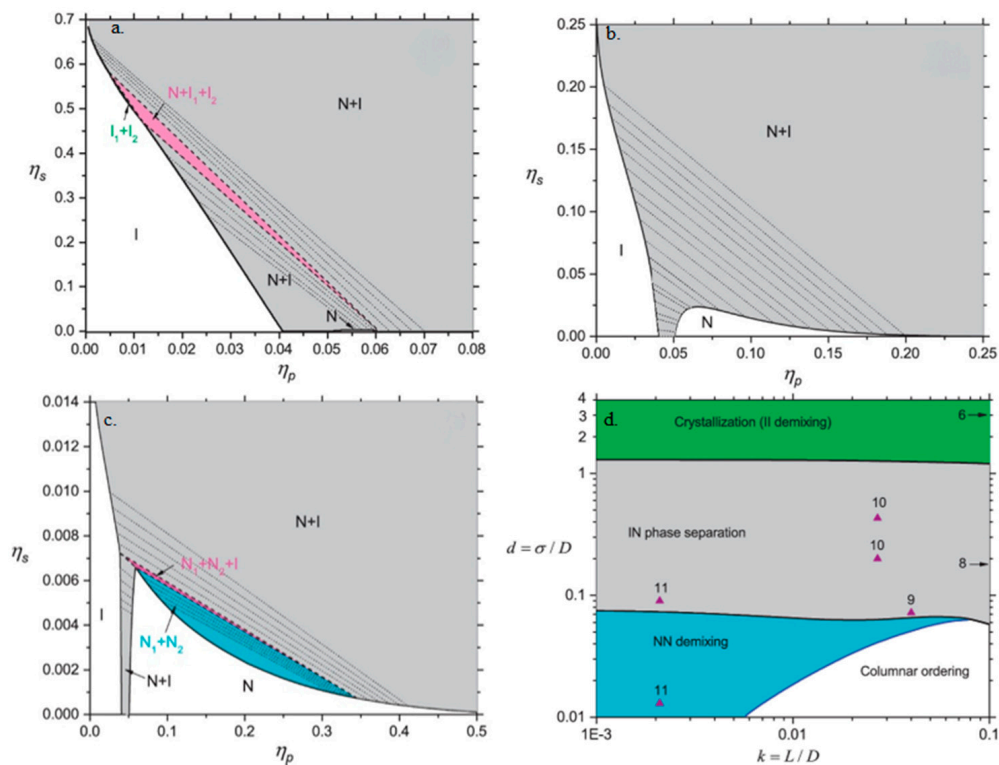


**Figure 14.** Effects of spheres on the phase behavior of platelets.  $\eta_s$  = fraction of spheres,  $\eta_p$  = fraction of platelets,  $\sigma$  = sphere diameter,  $D$  = platelet lateral diameter. In (a–c),  $k = L/D = 0.01$  and the coexisting isotropic (nematic) phases are labeled as  $I_1$  and  $I_2$  ( $N_1$  and  $N_2$ ). The two-phase and three-phase regions are indicated by gray (I–N), green ( $I_1$ – $I_2$ ), cyan ( $N_1$ – $N_2$ ), and pink ( $I_1$ – $N_1$ – $N_2$  and  $I_1$ – $I_2$ –N). (a)  $\sigma/D = 1.3$ , (b)  $\sigma/D = 0.2$ , and (c)  $\sigma/D = 0.03$ . (d) Phase diagrams of sphere-plate mixtures shown in the diameter ratio–aspect ratio ( $\sigma/D$ – $L/D$ ) plane. Regions of the phase diagrams are coloured differently: (1) The phase diagram is dominated by strong fractionation and reentrance of isotropic–nematic phase transition (gray), (2) the region of isotropic–nematic and isotropic–crystal transition, where the isotropic–isotropic demixing is not stable (green), (3) the region of nematic–nematic demixing and isotropic–nematic transition (cyan) and (4) those systems where the nematic–nematic demixing is unlikely to occur and is replaced by isotropic–columnar transition (white). The molecular parameters of some experimental systems are highlighted by triangle symbols and the numbers refer to their references. Modified from Aliabadi, R.; Moradi, R.; Varga, S. Tracking three-phase coexistences in binary mixtures of hard plates and spheres. *J. Chem. Phys.* 2016, 144, 074902, with the permission of AIP Publishing [111].

Understanding of the phase behavior of 2D–0D mixtures has improved significantly in the last five years. While there are some discrepancies based on the approach and whether the platelets are assumed to have finite thickness or be infinitely thin, there is general agreements that the ratio of the particle to platelet diameter is a key determinant of phase behavior. In addition, the absolute and relative concentrations have an influence. A key issue with experimental studies is the time scale of investigation since changes can occur over a year, and perhaps even longer. In addition, there are still many unanswered questions about the role of polydispersity and inter-particle interactions in both theoretical and experimental studies. Continuing to refine the understanding of these systems will facilitate controlled microstructure formation in dispersions that are suitable for coatings with desired microstructure and properties.

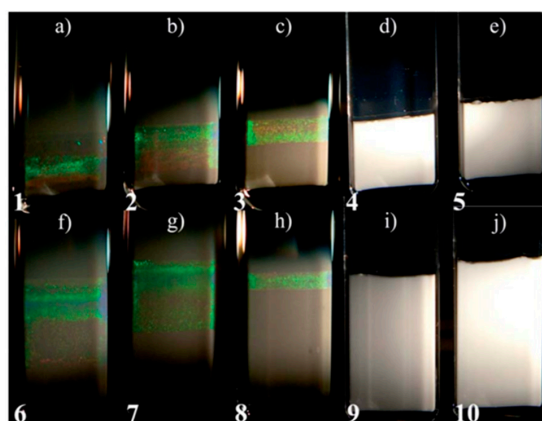


**Figure 15.** Samples of gibbsite/silica suspensions after one year of sedimentation. Samples (a–e) are 4 vol% gibbsite and 2, 3, 5, 7, and 8 vol% of silica particles, respectively. Samples (f–j) have 8 vol% gibbsite and 2, 3, 5, 7, and 8 vol% of silica particles, respectively. Reprinted with permission from Kleshchanok, D.; Meijer, J.-M.; Petukhov, A.V.; Portale, G.; Lekkerkerker, H.N.W. Sedimentation and depletion attraction directing glass and liquid crystal formation in aqueous platelet/sphere mixtures. *Soft Matter* 2012, 8, 191–197, The Royal Society of Chemistry.

### 5.3. Nanoplatelets and Nanocylinders (2D–1D)

There is growing interest in using systems such as CNT/graphene [117], CNT/MXene [118,119], silver nanowire/graphene [120], silver nanowire/MXene [121,122] and CNC/GO [123,124], and CNC/MXene [125] to create multifunctional materials. For example, Jalili et al. highlighted that combining liquid crystals of ultra-large GO in organic solvents with SWNT enabled multifunctional papers that had higher moduli than those containing only GO. This was due to the SWNT being able to bridge the gaps between the GO platelets [56]. In spite of this interest, the phase behavior and microstructure of mixtures of nanoplatelets and nanocylinders have been largely unaddressed.

Based on simulations, 2D–1D mixtures can form a biaxial phase (two directors oriented perpendicular to each other) which is not found in the pure components [126]. However, van der Kooij and Lekkerkerker found the biaxial phase was unstable in their investigation of boehmite nanocylinders with  $L/D = 10$  and gibbsite nanoplatelets with  $L/D = 15$ . Up to a total volume fraction of 0.3, macroscopic phase separation was complete after 24 h without biaxial phase formation. At higher concentrations of  $0.3 \leq \phi_{total} \leq 0.5$ , they found the very rich phase behavior shown in Figure 16. The macroscopic phase separation took 2 weeks, but their reproducibility was suggestive of thermodynamic equilibrium. The formation of up to five phases shows that due to its polydispersity, the system should not simply be viewed as a two-component system; for a system of two mesogens and the solvent, the Gibbs phase rule would have been violated. The authors noted that it is difficult to predict the phase behavior of cylinder-platelet systems due to the entropic contributions from orientation, excluded volume, and mixing [127].

Woolston and Duijneveldt found that combining montmorillonite (MMT) nanoplatelets with sepiolite (Sep) nanocylinders also showed complex phase behavior [128]. The aqueous MMT alone formed a gel, and aqueous Sep formed a nematic, but the addition of Sep to MMT could result in three-phase coexistence where the bottom layer consisted of a nematic Sep cylinder-rich phase, the middle layer consisted of an MMT platelet-rich phase, and the top layer was a dilute isotropic layer [128]. For all MMT concentrations above 1 vol%, however, the system gelled and the MMT concentration required for gelation decreased as the Sep concentration was increased to 4 vol%. The authors highlighted that their findings could be used in dispersion formulations to strengthen or weaken a gel phase; however, the effects of sepiolite on MMT gel strength were not rheologically quantified.

In contrast, ten Brinke et al. focused on the rheological properties of clay dispersions in a two-part work investigating platelets (gibbsite), cylinders (boehmite), and laths (hectorite) individually and then in binary mixtures [28,29]. Laths are distinct from platelets as they allow three different dimensions for the particle axis. The rheological behavior of the materials was characterized by oscillatory, transient, and steady shear flow pre-treated with a pre-shear and recovery protocol and modeled via a simple viscoelastic model [29]. Interestingly, these materials behave as elasto-viscous high viscosity solids at low strains and shear-thinning low viscosity liquids at high strains. However, there is a complex intermediate range defined as a “yield space” that accounts for sample microstructure of the sample as well as stress–strain–time history [29]. The mixtures generally demonstrated similar behavior to the pure components. In addition, the rheological properties were greater in magnitude when a small amount (0.25 wt%) of the second component is added to the first component in the dispersion. The shear storage and viscous moduli, effective viscosity, and yield stress were larger for the mixtures of the laths and platelets than the laths and cylinders [29]. The authors highlighted that a detailed model for explaining their results does not yet exist [29]. However, their results provide an important baseline and motivation for understanding 2D–1D systems with the goal of being able to formulate dispersions that possess both desirable microstructures and rheological properties suitable for processing solid coatings, fibers, or objects using a given manufacturing technique.

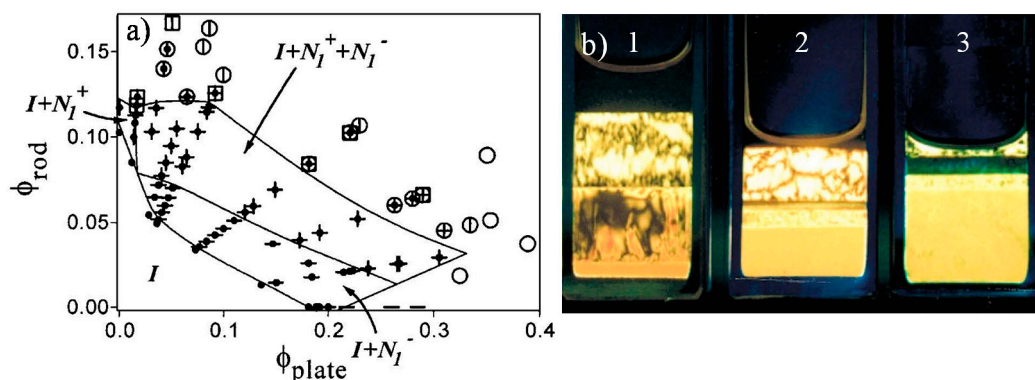


**Figure 16.** (a) Phase diagram for boehmite/gibbsite (nanocylinder/nanoplatelet).  $N^+$  indicates a nematic phase of predominantly nanocylinders, and  $N^-$  indicates a nematic phase of predominantly nanoplatelets. Filled circles indicate isotropic, vertical lines  $N_1^+$ , dashes  $N_1^-$ , open squares  $N_1^+$ , open circles  $N_2^-$ . (b) Polarized light images of concentrated dispersions of concentrations (boehmite, gibbsite) and top to bottom. (1) (0.06, 0.26)  $I + N_1^+ + N_1^- + N_2^-$ , (2) (0.10, 0.22)  $I + N_1^+ + N_2^+ N_1^- + N_2^-$ , (3) (0.07, 0.29)  $N_1^+ + N_2^+ N_1^- + N_2^-$ . Reprinted with permission from van der Kooij, F.M.; Lekkerkerker, H.N.W. Liquid-crystalline phase behavior of a colloidal rod-plate mixture. *Phys. Rev. Lett.* 2000, 84, 781–784. Copyright 2000 by the American Physical Society [127].

#### 5.4. Outlook for Understanding and Exploiting Shape Dispersity

Dispersions of nanomesogens of different shapes, and often different chemical compositions, are increasingly being studied to achieve desired thermal, mechanical, or electrical properties. They are also being studied to achieve the rheological properties required for processing by a given manufacturing method. Fundamental study of the phase behavior of shape disperse systems will lead to better understanding of both rheological properties and the ability to achieve solid materials with desirable microstructures. The behavior of 1D–0D systems is generally understood, particularly for monodisperse athermal systems. However, practical systems often also include size dispersity and thermodynamic interactions that further complicate phase behavior. Therefore, a concerted experimental and theoretical effort is needed. This is particularly necessary for 1D–2D and 2D–0D systems.

## 6. Conclusions and Future Directions

The last twenty years have resulted in a significant shift in lyotropic liquid crystalline science from focusing almost exclusively on polymeric mesogens to focusing on nanomesogens. Much has been achieved with respect to characterizing the phase behavior of individual systems, and computational studies have enabled significant advances in understanding the profound effects of size and shape dispersity on liquid crystalline phase behavior. While traditionally viewed as an annoyance, recent work suggests that polydispersity actually represents an opportunity to achieve a broader range of microstructures. There has been significant progress in evaluating size and shape dispersity separately, but much work needs to be done to understand real systems consisting of non-athermal interactions, size polydispersity, and shape polydispersity. This review provided highlights of experimental and theoretical work related to the phase behavior of polydisperse nanocylinders and nanoplatelets as well as binary mixtures of nanocylinder, nanoplatelets, and nanoparticles. A remarkable theme throughout the literature is the amazing robustness of the Onsager framework and how the initial investigations of TMV and vanadium pentoxide started a field that is still being explored today.

To date, traditional methods such as cross-polarized microscopy, rheology, and small angle x-ray scattering (SAXS) have been used to characterize nanomesogen systems. While these methods will continue to play a critical role in studying nanomesogen phase behavior, future advances in evaluating shape, size, and material disperse systems will be facilitated by the ongoing evolution of manufacturing technologies and characterization methods. Advanced scattering methods such as grazing incidence small angle x-ray and neutron scattering (GISAXS and GISANS) promise new insights into microstructure. Integrated spectroscopic and morphological methods such as Raman spectroscopy–atomic force microscopy (Raman–AFM) will enable detailed insights into how chemistry affects ordering in multicomponent systems. As new methodologies for dispersion processing such as ink jet printing, direct ink writing, and aerosol jet printing continue to evolve alongside traditional methods of film casting and solution spinning, the intersection of phase behavior and rheological properties need to be further studied to enable the production of materials with controlled microstructures. Phase behavior affects rheological properties, and quiescent dispersion microstructures can be deformed by both processing shear and solvent removal during solidification. Therefore, methods that examine the evolution of microstructure under shear such as rheo-optics, rheo-SALS (small angle light scattering), rheo-SAXS (small angle X-ray scattering), and rheo-SANS (small angle neutron scattering) will be critical to advancing both the fundamental science and applications of size and shape disperse lyotropic liquid crystals.

Increasing interest in multifunctional materials for electronics, energy storage, optics, sensors, mechanical structures, wearables, and biomedical devices will continue to drive research on both individual nanomaterials and mixtures of nanomaterials. Many of these will benefit from the anisotropic properties that can be achieved by exploiting lyotropic liquid crystalline phase behavior. Increased comprehension of how to tailor microstructure through size and shape dispersity is needed to enable the rational design of dispersions instead of the current trial and error approach. While significant advances have been made in the last ten years, the current models largely neglect the complexities of real systems that possess size polydispersity, shape polydispersity, and can have significant electrostatic or van der Waals interactions. In addition, the phase behavior of dispersions containing more than two components has yet to be addressed. Significant advancements and progress toward functional materials assembled from complex dispersions of nanomesogen building blocks will require ongoing theoretical advances and close collaboration between the theoretical and experimental soft matter communities.

**Author Contributions:** Conceptualization, V.A.D.; Writing–Original Draft Preparation, F.H., M.B.W., S.K.A., V.A.D.; Writing–Review and Editing, F.H., M.B.W., S.K.A., V.A.D.; Funding Acquisition, V.A.D. All authors have read and agreed to the published version of the manuscript.

**Funding:** The authors acknowledge funding from the US National Science Foundation Award (Grant CBET-2005413).

**Conflicts of Interest:** The authors declare no conflict of interest.

## References

1. Lagerwall, J.P.F.; Scalia, G. A new era for liquid crystal research: Applications of liquid crystals in soft matter nano-, bio- and microtechnology. *Curr. Appl. Phys.* **2012**, *12*, 1387–1412. [[CrossRef](#)]
2. Lekkerkerker, H.N.W.; Vroege, G.J. Liquid crystal phase transitions in suspensions of mineral colloids: new life from old roots. *Philos. Trans. R. Soc. A Math. Phys. Eng. Sci.* **2013**, *371*, 20120263. [[CrossRef](#)] [[PubMed](#)]
3. Livage, J.; Pelletier, O.; Davidson, P. Vanadium pentoxide sol and gel mesophases. *J. Sol-Gel Sci. Technol.* **2000**, *19*, 275–278. [[CrossRef](#)]
4. Sonin, A.S. Inorganic lyotropic liquid crystals. *J. Mater. Chem.* **1998**, *8*, 2557–2574. [[CrossRef](#)]
5. Stanley, W.M. Isolation of a crystalline protein possessing the properties of tobacco mosaic virus. *Science* **1935**, *81*, 644. [[CrossRef](#)]
6. Onsager, L. The effects of shape on the interaction of colloidal particles. *Ann. N.Y. Acad. Sci.* **1949**, *51*, 627–659. [[CrossRef](#)]
7. Davis, V.A. Liquid crystalline assembly of nanocylinders. *J. Mater. Res.* **2011**, *26*, 140–153. [[CrossRef](#)]
8. Solomon, M.J.; Spicer, P.T. Microstructural regimes of colloidal rod suspensions, gels, and glasses. *Soft Matter* **2010**, *6*, 1391–1400. [[CrossRef](#)]
9. Bakker, H.E.; Dussi, S.; Droste, B.L.; Besseling, T.H.; Kennedy, C.L.; Wiegant, E.I.; Liu, B.; Imhof, A.; Dijkstra, M.; van Blaaderen, A. Phase diagram of binary colloidal rod-sphere mixtures from a 3D real-space analysis of sedimentation–diffusion equilibria. *Soft Matter* **2016**, *12*, 9238–9245. [[CrossRef](#)]
10. Chen, M.; Li, H.; Chen, Y.; Mejia, A.; Wang, X.; Cheng, Z. Observation of isotropic-isotropic demixing in colloidal platelet-sphere mixtures. *Soft Matter* **2015**, *11*, 5775–5779. [[CrossRef](#)]
11. Kleshchanok, D.; Holmqvist, P.; Meijer, J.-M.; Lekkerkerker, H.N.W. Lyotropic Smectic B phase formed in suspensions of charged colloidal platelets. *J. Am. Chem. Soc.* **2012**, *134*, 5985–5990. [[CrossRef](#)] [[PubMed](#)]
12. Murali, S.; Xu, T.; Marshall, B.D.; Kayatin, M.J.; Pizarro, K.; Radhakrishnan, V.K.; Nepal, D.; Davis, V.A. Lyotropic liquid crystalline self-assembly in dispersions of silver nanowires and nanoparticles. *Langmuir* **2010**, *26*, 11176–11183. [[CrossRef](#)] [[PubMed](#)]
13. Lauffer, M.A. The size and shape of tobacco mosaic virus particles. *J. Am. Chem. Soc.* **1944**, *66*, 1188–1194. [[CrossRef](#)]
14. Tang, J.; Fraden, S. Isotropic-cholesteric phase transition in colloidal suspensions of filamentous bacteriophage fd. *Liq. Cryst.* **1995**, *19*, 459–467. [[CrossRef](#)]
15. Revol, J.F.; Bradford, H.; Giasson, J.; Marchessault, R.H.; Gray, D.G. Helicoidal self-ordering of cellulose microfibrils in aqueous suspension. *Int. J. Biol. Macromol.* **1992**, *14*, 170–172. [[CrossRef](#)]
16. Revol, J.F.; Godbout, L.; Dong, X.M.; Gray, D.G.; Chanzy, H.; Maret, G. Chiral nematic suspensions of cellulose crystallites—Phase-separation and magnetic-field orientation. *Liq. Cryst.* **1994**, *16*, 127–134. [[CrossRef](#)]
17. Reid, M.S.; Villalobos, M.; Cranston, E.D. Benchmarking cellulose nanocrystals: From the laboratory to industrial production. *Langmuir* **2017**, *33*, 1583–1598. [[CrossRef](#)]
18. Schütz, C.; Bruckner, J.R.; Honorato-Rios, C.; Tosheva, Z.; Anyfantakis, M.; Lagerwall, J.P. From equilibrium liquid crystal formation and kinetic arrest to photonic bandgap films using suspensions of cellulose nanocrystals. *Crystals* **2020**, *10*, 199. [[CrossRef](#)]
19. Fan, X.Z.; Pomerantseva, E.; Gnerlich, M.; Brown, A.; Gerasopoulos, K.; McCarthy, M.; Culver, J.; Ghodssi, R. Tobacco mosaic virus: A biological building block for micro/nano/biosystems. *J. Vac. Sci. Technol. A* **2013**, *31*, 050815. [[CrossRef](#)]
20. Gabriel, J.C.; Davidson, P. Mineral liquid crystals from self-assembly of anisotropic nanosystems. In *Colloid Chemistry I. Topics in Current Chemistry*; Antonietti, M., Ed.; Springer: Berlin/Heidelberg, Germany, 2003; Volume 226, pp. 119–172. [[CrossRef](#)]
21. Gabriel, J.C.P.; Davidson, P. New trends in colloidal liquid crystals based on mineral moieties. *Adv. Mater.* **2000**, *12*, 9–20. [[CrossRef](#)]
22. Ruzicka, B.; Zaccarelli, E. A fresh look at the laponite phase diagram. *Soft Matter* **2011**, *7*, 1268–1286. [[CrossRef](#)]
23. Vroege, G.J.; Thies-Weesie, D.M.E.; Petukhov, A.V.; Lemaire, B.J.; Davidson, P. Smectic liquid-crystalline order in suspensions of highly polydisperse goethite nanorods. *Adv. Mater.* **2006**, *18*, 2565–2568. [[CrossRef](#)]

24. Kleshchanok, D.; Meijer, J.-M.; Petukhov, A.V.; Portale, G.; Lekkerkerker, H.N.W. Attractive glass formation in aqueous mixtures of colloidal gibbsite platelets and silica spheres. *Soft Matter* **2011**, *7*, 2832–2840. [[CrossRef](#)]
25. Mourad, M.C.D.; Byelov, D.V.; Petukhov, A.V.; Matthijs de Winter, D.A.; Verkleij, A.J.; Lekkerkerker, H.N.W. Sol–gel transitions and liquid crystal phase transitions in concentrated aqueous suspensions of colloidal gibbsite platelets. *J. Phys. Chem. B* **2009**, *113*, 11604–11613. [[CrossRef](#)] [[PubMed](#)]
26. Mourad, M.C.D.; Wijnhoven, J.E.G.J.; van't Zand, D.D.; van der Beek, D.; Lekkerkerker, H.N.W. Gelation versus liquid crystal phase transitions in suspensions of plate-like particles. *Philos. Trans. R. Soc. A Math. Phys. Eng. Sci.* **2006**, *364*, 2807–2816. [[CrossRef](#)]
27. Prestidge, C.A.; Ametov, I.; Addai-Mensah, J. Rheological investigations of gibbsite particles in synthetic bayer liquors. *Coll. Surf. A Physiochem. Eng. Asp.* **1999**, *157*, 137–145. [[CrossRef](#)]
28. ten Brinke, A.J.W.; Bailey, L.; Lekkerkerker, H.N.W.; Maitland, G.C. Rheology modification in mixed shape colloidal dispersions. Part I: Pure components. *Soft Matter* **2007**, *3*, 1145–1162. [[CrossRef](#)]
29. ten Brinke, A.J.W.; Bailey, L.; Lekkerkerker, H.N.W.; Maitland, G.C. Rheology modification in mixed shape colloidal dispersions. Part ii: Mixtures. *Soft Matter* **2008**, *4*, 337–348. [[CrossRef](#)]
30. van der Beek, D.; Lekkerkerker, H.N.W. Liquid crystal phases of charged colloidal platelets. *Langmuir* **2004**, *20*, 8582–8586. [[CrossRef](#)]
31. Verhoeff, A.A.; Wensink, H.H.; Vis, M.; Jackson, G.; Lekkerkerker, H.N.W. Liquid crystal phase transitions in systems of colloidal platelets with bimodal shape distribution. *J. Phys. Chem. B* **2009**, *113*, 13476–13484. [[CrossRef](#)]
32. Xu, T.; Davis, V.A. Liquid crystalline phase behavior of silica nanorods in dimethyl sulfoxide and water. *Langmuir* **2014**, *30*, 4806–4813. [[CrossRef](#)] [[PubMed](#)]
33. Wang, J.M.; Khoo, E.; Lee, P.S.; Ma, J. Synthesis, assembly, and electrochromic properties of uniform crystalline WO<sub>3</sub> nanorods. *J. Phys. Chem. C* **2008**, *112*, 14306–14312. [[CrossRef](#)]
34. Li, L.-S.; Alivisatos, A.P. Semiconductor nanorod liquid crystals and their assembly on a substrate. *Adv. Mater.* **2003**, *15*, 408–411. [[CrossRef](#)]
35. Yang, X.; He, W.; Wang, S.; Zhou, G.; Tang, Y.; Yang, J. Effect of the different shapes of silver particles in conductive ink on electrical performance and microstructure of the conductive tracks. *J. Mater. Sci. Mater. Electron.* **2012**, *23*, 1980–1986. [[CrossRef](#)]
36. Dessombz, A.; Chiche, D.; Davidson, P.; Panine, P.; Chanéac, C.; Jolivet, J.-P. Design of liquid-crystalline aqueous suspensions of rutile nanorods: Evidence of anisotropic photocatalytic properties. *J. Am. Chem. Soc.* **2007**, *129*, 5904–5909. [[CrossRef](#)] [[PubMed](#)]
37. Jana, N.R.; Gearheart, L.A.; Obare, S.O.; Johnson, C.J.; Edler, K.J.; Mann, S.; Murphy, C.J. Liquid crystalline assemblies of ordered gold nanorods. *J. Mater. Chem.* **2002**, *12*, 2909–2912. [[CrossRef](#)]
38. Nikoobakht, B.; Wang, Z.L.; El-Sayed, M.A. Self-assembly of gold nanorods. *J. Phys. Chem. B* **2000**, *104*, 8635–8640. [[CrossRef](#)]
39. Reibold, M.; Paufler, P.; Levin, A.A.; Kochmann, W.; Patzke, N.; Meyer, D.C. Materials: Carbon nanotubes in an ancient Damascus sabr. *Nature* **2006**, *444*, 286. [[CrossRef](#)]
40. Akbari, A.; Sheath, P.; Martin, S.T.; Shinde, D.B.; Shaibani, M.; Banerjee, P.C.; Tkacz, R.; Bhattacharyya, D.; Majumder, M. Large-area graphene-based nanofiltration membranes by shear alignment of discotic nematic liquid crystals of graphene oxide. *Nat. Commun.* **2016**, *7*, 10891. [[CrossRef](#)]
41. Dan, B.; Behabtu, N.; Martinez, A.; Evans, J.S.; Kosynkin, D.V.; Tour, J.M.; Pasquali, M.; Smalyukh, I.I. Liquid crystals of aqueous, giant graphene oxide flakes. *Soft Matter* **2011**, *7*, 11154–11159. [[CrossRef](#)]
42. Liu, Y.; Xu, Z.; Gao, W.; Cheng, Z.; Gao, C. Graphene and other 2D colloids: Liquid crystals and macroscopic fibers. *Adv. Mater.* **2017**, *29*, 1606794-n/a. [[CrossRef](#)] [[PubMed](#)]
43. Xu, Z.; Gao, C. Graphene in macroscopic order: Liquid crystals and wet-spun fibers. *Acc. Chem. Res.* **2014**, *47*, 1267–1276. [[CrossRef](#)] [[PubMed](#)]
44. Zakri, C.; Blanc, C.; Grelet, E.; Zamora-Ledezma, C.; Puech, N.; Anglaret, E.; Poulin, P. Liquid crystals of carbon nanotubes and graphene. *Philos. Trans. R. Soc. A Math. Phys. Eng. Sci.* **2013**, *371*. [[CrossRef](#)] [[PubMed](#)]
45. Green, M.J.; Parra-Vasquez, A.N.G.; Behabtu, N.; Pasquali, M. Modeling the phase behavior of polydisperse rigid rods with attractive interactions with applications to single-walled carbon nanotubes in superacids. *J. Chem. Phys.* **2009**, *131*, 041401. [[CrossRef](#)] [[PubMed](#)]

46. Behabtu, N.; Lomeda, J.R.; Green, M.J.; Higginbotham, A.L.; Sinitiskii, A.; Kosynkin, D.V.; Tsentlovich, D.; Parra-Vasquez, A.N.G.; Schmidt, J.; Kesselman, E. Spontaneous high-concentration dispersions and liquid crystals of graphene. *Nat. Nanotechnol.* **2010**, *5*, 406–411. [[CrossRef](#)]
47. Davis, V.A.; Ericson, L.M.; Parra-Vasquez, A.N.G.; Fan, H.; Wang, Y.; Prieto, V.; Longoria, J.A.; Ramesh, S.; Saini, R.K.; Kittrell, C.; et al. Phase behavior and rheology of SWNTs in superacids. *Macromolecules* **2004**, *37*, 154–160. [[CrossRef](#)]
48. Moulton, S.E.; Maugey, M.; Poulin, P.; Wallace, G.G. Liquid crystal behavior of single-walled carbon nanotubes dispersed in biological hyaluronic acid solutions. *J. Am. Chem. Soc.* **2007**, *129*, 9452–9457. [[CrossRef](#)]
49. Barisci, J.N.; Tahhan, M.; Wallace, G.G.; Badaire, S.; Vaugien, T.; Maugey, M.; Poulin, P. Properties of carbon nanotube fibers spun from DNA-stabilized dispersions. *Adv. Funct. Mater.* **2004**, *14*, 133–138. [[CrossRef](#)]
50. Bergin, S.D.; Nicolosi, V.; Giordani, S.; de Gromard, A.; Carpenter, L.; Blau, W.J.; Coleman, J.N. Exfoliation in ecstasy: Liquid crystal formation and concentration-dependent debundling observed for single-wall nanotubes dispersed in the liquid drug  $\gamma$ -butyrolactone. *Nanotechnology* **2007**, *18*, 455705. [[CrossRef](#)]
51. Ao, G.; Nepal, D.; Aono, M.; Davis, V.A. Cholesteric and nematic liquid crystalline phase behavior of double-stranded DNA stabilized single-walled carbon nanotube dispersions. *ACS Nano* **2011**, *5*, 1450–1458. [[CrossRef](#)]
52. Song, W.; Kinloch, I.A.; Windle, A.H. Nematic liquid crystallinity of multiwall carbon nanotubes. *Science* **2003**, *302*, 1363. [[CrossRef](#)]
53. Song, Y.S.; Youn, J.R. Influence of dispersion states of carbon nanotubes on physical properties of epoxy nanocomposites. *Carbon* **2005**, *43*, 1378–1385. [[CrossRef](#)]
54. Gudarzi, M.M. Colloidal stability of graphene oxide: Aggregation in two dimensions. *Langmuir* **2016**, *32*, 5058–5068. [[CrossRef](#)]
55. Paredes, J.I.; Villar-Rodil, S.; Martinez-Alonso, A.; Tascon, J.M.D. Graphene oxide dispersions in organic solvents. *Langmuir* **2008**, *24*, 10560–10564. [[CrossRef](#)] [[PubMed](#)]
56. Jalili, R.; Aboutalebi, S.H.; Esrafilzadeh, D.; Konstantinov, K.; Moulton, S.E.; Razal, J.M.; Wallace, G.G. Organic solvent-based graphene oxide liquid crystals: A facile route toward the next generation of self-assembled layer-by-layer multifunctional 3D architectures. *ACS Nano* **2013**, *7*, 3981–3990. [[CrossRef](#)] [[PubMed](#)]
57. Ahmad, R.T.M.; Hong, S.-H.; Shen, T.-Z.; Masud, A.R.; Song, J.-K. Effect of solvents on the electro-optical switching of graphene oxide dispersions. *Appl. Phys. Lett.* **2016**, *108*, 251903. [[CrossRef](#)]
58. Naficy, S.; Jalili, R.; Aboutalebi, S.H.; Gorkin, R.A.; Konstantinov, K.; Innis, P.C.; Spinks, G.M.; Poulin, P.; Wallace, G.G. Graphene oxide dispersions: Tuning rheology to enable fabrication. *Mater. Horiz.* **2014**, *1*, 326–331. [[CrossRef](#)]
59. Liu, Y.; Chen, C.M.; Liu, L.Y.; Zhu, G.R.; Kong, Q.Q.; Hao, R.X.; Tan, W. Rheological behavior of high concentrated dispersions of graphite oxide. *Soft Mater.* **2015**, *13*, 167–175. [[CrossRef](#)]
60. Jalili, R.; Aboutalebi, S.H.; Esrafilzadeh, D.; Shepherd, R.L.; Chen, J.; Aminorroaya-Yamini, S.; Konstantinov, K.; Minett, A.I.; Razal, J.M.; Wallace, G.G. Scalable one-step wet-spinning of graphene fibers and yarns from liquid crystalline dispersions of graphene oxide: Towards multifunctional textiles. *Adv. Funct. Mater.* **2013**, *23*, 5345–5354. [[CrossRef](#)]
61. Aboutalebi, S.H.; Gudarzi, M.M.; Zheng, Q.B.; Kim, J.K. Spontaneous formation of liquid crystals in ultralarge graphene oxide dispersions. *Adv. Funct. Mater.* **2011**, *21*, 2978–2988. [[CrossRef](#)]
62. Andrienko, D. Introduction to liquid crystals. *J. Mol. Liq.* **2018**, *267*, 520–541. [[CrossRef](#)]
63. Veerman, J.A.C.; Frenkel, D. Phase behavior of disklike hard-core mesogens. *Phys. Rev. A* **1992**, *45*, 5632–5648. [[CrossRef](#)] [[PubMed](#)]
64. Khokhlov, A.R. Theories based on the Onsager approach. In *Liquid Crystallinity in Polymers*; Ciferri, A., Ed.; VCH Publishers: New York, NY, USA, 1991; pp. 97–129.
65. Doi, M.; Edwards, S.F. *The Theory of Polymer Dynamics*; Oxford University Press: Oxford, UK, 1986.
66. Roij, R.V. The isotropic and nematic liquid crystal phase of colloidal rods. *Eur. J. Phys.* **2005**, *26*, S57–S67. [[CrossRef](#)]
67. Larson, R.G. *The Structure and Rheology of Complex Fluids*; Oxford University Press: New York, NY, USA, 1999.
68. Zhang, S.; Kinloch, I.A.; Windle, A.H. Mesogenicity drives fractionation in lyotropic aqueous suspensions of multiwall carbon nanotubes. *Nano Lett.* **2006**, *6*, 568–572. [[CrossRef](#)] [[PubMed](#)]

69. Davis, V.A.; Parra-Vasquez, A.N.G.; Green, M.J.; Rai, P.K.; Behabtu, N.; Prieto, V.; Booker, R.D.; Schmidt, J.; Kesselman, E.; Zhou, W.; et al. True solutions of single-walled carbon nanotubes for assembly into macroscopic materials. *Nat. Nanotechnol.* **2009**, *4*, 830–834. [[CrossRef](#)] [[PubMed](#)]
70. Ziegler, K.J.; Rauwald, U.; Gu, Z.; Liang, F.; Billups, W.; Hauge, R.H.; Smalley, R.E. Statistically accurate length measurements of single-walled carbon nanotubes. *J. Nanosci. Nanotechnol.* **2007**, *7*, 2917–2921. [[CrossRef](#)]
71. Parra-Vasquez, A.N.G.; Stepanek, I.; Davis, V.A.; Moore, V.C.; Haroz, E.H.; Shaver, J.; Hauge, R.H.; Smalley, R.E.; Pasquali, M. Simple length determination of single-walled carbon nanotubes by viscosity measurements in dilute suspensions. *Macromolecules* **2007**, *40*, 4043–4047. [[CrossRef](#)]
72. Pagani, G.; Green, M.J.; Poulin, P.; Pasquali, M. Competing mechanisms and scaling laws for carbon nanotube scission by ultrasonication. *Proc. Natl. Acad. Sci. USA* **2012**, *109*, 11599. [[CrossRef](#)]
73. Moon, R.J.; Martini, A.; Nairn, J.; Simonsen, J.; Youngblood, J. Cellulose nanomaterials review: Structure, properties and nanocomposites. *Chem. Soc. Rev.* **2011**, *40*, 3941–3994. [[CrossRef](#)]
74. Elazzouzi-Hafraoui, S.; Nishiyama, Y.; Putaux, J.-L.; Heux, L.; Dubreuil, F.; Rochas, C. The shape and size distribution of crystalline nanoparticles prepared by acid hydrolysis of native cellulose. *Biomacromolecules* **2008**, *9*, 57–65. [[CrossRef](#)]
75. Beck-Candanedo, S.; Roman, M.; Gray, D.G. Effect of reaction conditions on the properties and behavior of wood cellulose nanocrystal suspensions. *Biomacromolecules* **2005**, *6*, 1048–1054. [[CrossRef](#)] [[PubMed](#)]
76. Adams, M.; Fraden, S. Phase behavior of mixtures of rods (tobacco mosaic virus) and spheres (polyethylene oxide, bovine serum albumin). *Biophys. J.* **1998**, *74*, 669–677. [[CrossRef](#)]
77. Bates, M.A.; Frenkel, D. Influence of polydispersity on the phase behavior of colloidal liquid crystals: A monte carlo simulation study. *J. Chem. Phys.* **1998**, *109*, 6193–6199. [[CrossRef](#)]
78. Woolston, P.; van Duijneveldt, J.S. Isotropic-nematic phase transition of polydisperse clay rods. *J. Chem. Phys.* **2015**, *142*, 184901. [[CrossRef](#)] [[PubMed](#)]
79. Donald, A.M.; Windle, A.H.; Hanna, S. Theories of liquid crystallinity in polymers. In *Liquid Crystalline Polymers*, 2nd ed.; Windle, A.H., Donald, A.M., Hanna, S., Eds.; Cambridge University Press: Cambridge, UK, 2006; pp. 133–228. [[CrossRef](#)]
80. Honorato-Rios, C.; Lehr, C.; Schütz, C.; Sanctuary, R.; Osipov, M.A.; Baller, J.; Lagerwall, J.P.F. Fractionation of cellulose nanocrystals: Enhancing liquid crystal ordering without promoting gelation. *NPG Asia Mater.* **2018**, *10*, 455–465. [[CrossRef](#)]
81. Lekkerkerker, H.N.W.; Coulon, P.; Van Der Haegen, R.; Deblieck, R. On the isotropic-liquid crystal phase separation in a solution of rodlike particles of different lengths. *J. Chem. Phys.* **1984**, *80*, 3427–3433. [[CrossRef](#)]
82. Flory, P.J.; Abe, A. Statistical thermodynamics of mixtures of rodlike particles. 1. Theory for polydisperse systems. *Macromolecules* **1978**, *11*, 1119–1122. [[CrossRef](#)]
83. Flory, P.J. Phase equilibria in solutions of rod-like particles. *Proc. R. Soc. Lond. Ser. A Math. Phys. Sci.* **1956**, *234*, 73–89. [[CrossRef](#)]
84. Vroege, G.J.; Lekkerkerker, H.N.W. Theory of the isotropic-nematic-nematic phase separation for a solution of bidisperse rodlike particles. *J. Chem. Phys.* **1993**, *97*, 3601–3605. [[CrossRef](#)]
85. Donald, A.M.; Windle, A.H. *Liquid Crystalline Polymers*; Cambridge University Press: Cambridge, UK, 1992.
86. Itou, T.; Teramoto, A. Multi-phase equilibrium in aqueous solutions of the triple-helical polysaccharide, schizophyllan. *Polym. J.* **1984**, *16*, 779–790. [[CrossRef](#)]
87. Kajiwara, K.; Donkai, N.; Hiragi, Y.; Inagaki, H. Lyotropic mesophase of imogolite, 1. Effect of polydispersity on phase diagram. *Die Makromol. Chem.* **1986**, *187*, 2883–2893. [[CrossRef](#)]
88. Buining, P.A.; Lekkerkerker, H.N.W. Isotropic-nematic phase separation of a dispersion of organophilic boehmite rods. *J. Chem. Phys.* **1993**, *97*, 11510–11516. [[CrossRef](#)]
89. Speranza, A.; Sollich, P. Simplified onsager theory for isotropic–nematic phase equilibria of length polydisperse hard rods. *J. Chem. Phys.* **2002**, *117*, 5421–5436. [[CrossRef](#)]
90. Speranza, A.; Sollich, P. Isotropic-nematic phase equilibria in the Onsager theory of hard rods with length polydispersity. *Phys. Rev. E* **2003**, *67*. [[CrossRef](#)] [[PubMed](#)]
91. Speranza, A.; Sollich, P. Isotropic-nematic phase equilibria of polydisperse hard rods: The effect of fat tails in the length distribution. *J. Chem. Phys.* **2003**, *118*, 5213–5223. [[CrossRef](#)]
92. van der Kooij, F.M.; Lekkerkerker, H.N.W. Formation of nematic liquid crystals in suspensions of hard colloidal platelets. *J. Chem. Phys. B* **1998**, *102*, 7829–7832. [[CrossRef](#)]

93. Gabriel, J.-C.P.; Sanchez, C.; Davidson, P. Observation of nematic liquid-crystal textures in aqueous gels of smectite clays. *J. Chem. Phys.* **1996**, *100*, 11139–11143. [[CrossRef](#)]
94. Jalili, R.; Aboutalebi, S.H.; Esrafilzadeh, D.; Konstantinov, K.; Razal, J.M.; Moultona, S.E.; Wallace, G.G. Formation and processability of liquid crystalline dispersions of graphene oxide. *Mater. Horiz.* **2014**, *1*, 87–91. [[CrossRef](#)]
95. Pusey, P.N.; Fijnaut, H.M.; Vrij, A. Mode amplitudes in dynamic light scattering by concentrated liquid suspensions of polydisperse hard spheres. *J. Chem. Phys.* **1982**, *77*, 4270–4281. [[CrossRef](#)]
96. Ahmad, R.T.M.; Hong, S.-H.; Shen, T.-Z.; Song, J.-K. Optimization of particle size for high birefringence and fast switching time in electro-optical switching of graphene oxide dispersions. *Opt. Express* **2015**, *23*, 4435–4440. [[CrossRef](#)]
97. Dogic, Z.; Sharma, Z.; Zakhary, M.J. Hypercomplex liquid crystals. *Annu. Rev. Condens. Matter Phys.* **2014**, *5*, 137–157. [[CrossRef](#)]
98. Asakura, S.; Oosawa, F. On interaction between two bodies immersed in a solution of macromolecules. *J. Chem. Phys.* **1954**, *22*, 1255–1256. [[CrossRef](#)]
99. Mao, Y.; Cates, M.E.; Lekkerkerker, H.N.W. Depletion force in colloidal systems. *Phys. A Stat. Mech. Its Appl.* **1995**, *222*, 10–24. [[CrossRef](#)]
100. Horn, D.W.; Ao, G.; Maugey, M.; Zakri, C.; Poulin, P.; Davis, V.A. Dispersion state and fiber toughness: Antibacterial lysozyme-single walled carbon nanotubes. *Adv. Funct. Mater.* **2013**, *23*, 6082–6090. [[CrossRef](#)]
101. Koenderink, G.H.; Vliegthart, G.A.; Kluijtmans, S.G.J.M.; van Blaaderen, A.; Philipse, A.P.; Lekkerkerker, H.N.W. Depletion-induced crystallization in colloidal rod–sphere mixtures. *Langmuir* **1999**, *15*, 4693–4696. [[CrossRef](#)]
102. Asakura, S.; Oosawa, F. Interaction between particles suspended in solutions of macromolecules. *J. Polym. Sci.* **1958**, *33*, 183–192. [[CrossRef](#)]
103. Dogic, Z.; Frenkel, D.; Fraden, S. Enhanced stability of layered phases in parallel hard spherocylinders due to addition of hard spheres. *Phys. Rev. E* **2000**, *62*, 3925–3933. [[CrossRef](#)]
104. Adams, M.; Dogic, Z.; Keller, S.L.; Fraden, S. Entropically driven microphase transitions in mixtures of colloidal rods and spheres. *Nature* **1998**, *393*, 349–352. [[CrossRef](#)]
105. Urakami, N.; Imai, M. Dependence on sphere size of the phase behavior of mixtures of rods and spheres. *J. Chem. Phys.* **2003**, *119*, 2463–2470. [[CrossRef](#)]
106. Xu, T.; Davis, V.A. Rheology and shear-induced textures of silver nanowire lyotropic liquid crystals. *J. Nanomater.* **2015**, *2015*, 9. [[CrossRef](#)]
107. Green, M.J. Isotropic–nematic phase separation and demixing in mixtures of spherical nanoparticles with length-polydisperse nanorods. *J. Polym. Sci. Part B Polym. Phys.* **2012**, *50*, 1321–1327. [[CrossRef](#)]
108. Lüders, A.; Siems, U.; Nielaba, P. Dynamic ordering of driven spherocylinders in a nonequilibrium suspension of small colloidal spheres. *Phys. Rev. E* **2019**, *99*, 022601. [[CrossRef](#)] [[PubMed](#)]
109. Wu, L.; Malijevský, A.; Avendaño, C.; Müller, E.A.; Jackson, G. Demixing, surface nematization, and competing adsorption in binary mixtures of hard rods and hard spheres under confinement. *J. Chem. Phys.* **2018**, *148*, 164701. [[CrossRef](#)] [[PubMed](#)]
110. Wu, L.; Malijevský, A.; Jackson, G.; Müller, E.A.; Avendaño, C. Orientational ordering and phase behaviour of binary mixtures of hard spheres and hard spherocylinders. *J. Chem. Phys.* **2015**, *143*, 044906. [[CrossRef](#)]
111. Aliabadi, R.; Moradi, R.; Varga, S. Tracking three-phase coexistences in binary mixtures of hard plates and spheres. *J. Chem. Phys.* **2016**, *144*, 074902. [[CrossRef](#)]
112. Harnau, L.; Dietrich, S. Bulk and wetting phenomena in a colloidal mixture of hard spheres and platelets. *Phys. Rev. E* **2005**, *71*, 011504. [[CrossRef](#)]
113. Oversteegen, S.M.; Lekkerkerker, H.N.W. Phase diagram of mixtures of hard colloidal spheres and discs: A free-volume scaled-particle approach. *J. Chem. Phys.* **2004**, *120*, 2470–2474. [[CrossRef](#)]
114. de las Heras, D.; Schmidt, M. Bulk fluid phase behaviour of colloidal platelet-sphere and platelet-polymer mixtures. *Philos. Trans. R. Soc. A Math. Phys. Eng. Sci.* **2013**, *371*. [[CrossRef](#)]
115. Kleshchanok, D.; Meijer, J.-M.; Petukhov, A.V.; Portale, G.; Lekkerkerker, H.N.W. Sedimentation and depletion attraction directing glass and liquid crystal formation in aqueous platelet/sphere mixtures. *Soft Matter* **2012**, *8*, 191–197. [[CrossRef](#)]
116. Sui, J. Stratification in the dynamics of sedimenting colloidal platelet–sphere mixtures. *Soft Matter* **2019**, *15*, 4714–4722. [[CrossRef](#)]

117. Lu, H.; Zhang, J.; Luo, J.; Gong, W.; Li, C.; Li, Q.; Zhang, K.; Hu, M.; Yao, Y. Enhanced thermal conductivity of free-standing 3D hierarchical carbon nanotube-graphene hybrid paper. *Compos. Part A Appl. Sci.* **2017**, *102*, 1–8. [[CrossRef](#)]
118. Zhao, M.Q.; Ren, C.E.; Ling, Z.; Lukatskaya, M.R.; Zhang, C.; Van Aken, K.L.; Barsoum, M.W.; Gogotsi, Y. Flexible MXene/carbon nanotube composite paper with high volumetric capacitance. *Adv. Mater.* **2015**, *27*, 339–345. [[CrossRef](#)] [[PubMed](#)]
119. Chen, H.; Yu, L.; Lin, Z.; Zhu, Q.; Zhang, P.; Qiao, N.; Xu, B. Carbon nanotubes enhance flexible MXene films for high-rate supercapacitors. *J. Mater. Sci.* **2020**, *55*, 1148–1156. [[CrossRef](#)]
120. Ricciardulli, A.G.; Yang, S.; Wetzelaer, G.J.A.; Feng, X.; Blom, P.W. Hybrid silver nanowire and graphene-based solution-processed transparent electrode for organic optoelectronics. *Adv. Funct. Mater.* **2018**, *28*, 1706010. [[CrossRef](#)]
121. Tang, H.; Feng, H.; Wang, H.; Wan, X.; Liang, J.; Chen, Y. Highly conducting MXene–silver nanowire transparent electrodes for flexible organic solar cells. *ACS Appl. Mater. Interfaces* **2019**, *11*, 25330–25337. [[CrossRef](#)]
122. Chen, W.; Liu, L.-X.; Zhang, H.-B.; Yu, Z.-Z. Flexible, transparent and conductive Ti<sub>3</sub>C<sub>2</sub>T<sub>x</sub> MXene-silver nanowire films with smart acoustic sensitivity for high-performance electromagnetic interference shielding. *ACS Nano* **2020**. [[CrossRef](#)]
123. Chen, L.; Hou, X.; Song, N.; Shi, L.; Ding, P. Cellulose/graphene bioplastic for thermal management: Enhanced isotropic thermally conductive property by three-dimensional interconnected graphene aerogel. *Compos. Part A Appl. Sci.* **2018**, *107*, 189–196. [[CrossRef](#)]
124. Chen, Q.; Liu, P.; Sheng, C.; Zhou, L.; Duan, Y.; Zhang, J. Tunable self-assembly structure of graphene oxide/cellulose nanocrystal hybrid films fabricated by vacuum filtration technique. *RSC Adv.* **2014**, *4*, 39301–39304. [[CrossRef](#)]
125. Tian, W.; VahidMohammadi, A.; Reid, M.S.; Wang, Z.; Ouyang, L.; Erlandsson, J.; Pettersson, T.; Wågberg, L.; Beidaghi, M.; Hamed, M.M. Multifunctional nanocomposites with high strength and capacitance using 2D MXene and 1D nanocellulose. *Adv. Mater.* **2019**, *31*, 1902977. [[CrossRef](#)]
126. van Roij, R.; Mulder, B. Demixing in a hard-plate mixture. *J. Phys. II* **1994**, *4*, 1763–1769. [[CrossRef](#)]
127. van der Kooij, F.M.; Lekkerkerker, H.N.W. Liquid-crystalline phase behavior of a colloidal rod-plate mixture. *Phys. Rev. Lett.* **2000**, *84*, 781–784. [[CrossRef](#)] [[PubMed](#)]
128. Woolston, P.; van Duijneveldt, J.S. Three-phase coexistence in colloidal rod-plate mixtures. *Langmuir* **2015**, *31*, 9290–9295. [[CrossRef](#)] [[PubMed](#)]



© 2020 by the authors. Licensee MDPI, Basel, Switzerland. This article is an open access article distributed under the terms and conditions of the Creative Commons Attribution (CC BY) license (<http://creativecommons.org/licenses/by/4.0/>).